2005-09

Direct imaging of minority charge carrier transport in luminescent semiconductors

Luber, David R.

Monterey, California. Naval Postgraduate School

NAVAL POSTGRADUATE SCHOOL

MONTEREY, CALIFORNIA

THESIS

DIRECT IMAGING OF MINORITY CHARGE CARRIER TRANSPORT IN LUMINESCENT SEMICONDUCTORS

by

David R. Luber

September 2005

Thesis Advisor:	Nancy M. Haegel
Co-Advisor:	Sherif Michael

Approved for public release; distribution is unlimited

THIS PAGE INTENTIONALLY LEFT BLANK

REPORT DOCUMENTATION PAGE			Form Approved OMB No. 0704-0188
Public reporting burden for this collection of information is estimated to average 1 hour per response, including the time for reviewing instruction, searching existing data sources, gathering and maintaining the data needed, and completing and reviewing the collection of information. Send comments regarding this burden estimate or any other aspect of this collection of information, including suggestions for reducing this burden, to Washington headquarters Services, Directorate for Information Operations and Reports, 1215 Jefferson Davis Highway, Suite 1204, Arlington, VA 22202-4302, and to the Office of Management and Budget, Paperwork Reduction Project (0704-0188) Washington DC 20503.			
1. AGENCY USE ONLY ***(Leave blank)***	**2. REPORT DATE** September 2005	**3. REPORT TYPE AND DATES COVERED** Master's Thesis	
4. TITLE AND SUBTITLE: Direct Imaging of Minority Charge Carrier Transport in Luminescent Semiconductors		**5. FUNDING NUMBERS**	
6. AUTHOR(S) David R. Luber			
7. PERFORMING ORGANIZATION NAME(S) AND ADDRESS(ES) Naval Postgraduate School Monterey, CA 93943-5000		**8. PERFORMING ORGANIZATION REPORT NUMBER**	
9. SPONSORING /MONITORING AGENCY NAME(S) AND ADDRESS(ES) Space and Naval Warfare Systems Center 53560 Hull Street San Diego, California 92152-5001		**10. SPONSORING/MONITORING AGENCY REPORT NUMBER**	
11. SUPPLEMENTARY NOTES The views expressed in this thesis are those of the author and do not reflect the official policy or position of the Department of Defense or the U.S. Government.			
12a. DISTRIBUTION / AVAILABILITY STATEMENT Approved for public release; distribution is unlimited		**12b. DISTRIBUTION CODE**	

13. ABSTRACT (maximum 200 words)

A quantitative method for extracting minority carrier diffusion and drift lengths is developed and demonstrated in a heavily-doped semiconductor heterostructure. This method advances the high resolution transport imaging technique, yielding key material parameters with a single, non-destructive measurement. This is the first demonstration of an SEM-based, contact-free, non-destructive technique for high-resolution minority carrier lifetime measurement. The measured values are in excellent agreement with theoretical calculations.

The imaging transport technique is also employed to image the nature of the generation region as a function of beam energy, probe current and sample atomic number. These types of images should be useful to allow for experimental verification of resolution limits in CL and EBIC associated with interaction volume effects in bulk materials and can be obtained without additional sample preparation.

Finally, several suggestions for further research are offered, including mapping of radiation damage in solar cells, near-contact E field mapping and studies of low-dimensional structures such as superlattices and quantum wires. These nanoscale structures are poised to usher-in the next revolution in solid-state electronic devices.

14. SUBJECT TERMS Contact-less measurements, Diffusion, Drift, Semiconductors, Transport Imaging, Minority carrier mobility, Minority carrier lifetime, Generation volume			**15. NUMBER OF PAGES** 74
			16. PRICE CODE
17. SECURITY CLASSIFICATION OF REPORT Unclassified	**18. SECURITY CLASSIFICATION OF THIS PAGE** Unclassified	**19. SECURITY CLASSIFICATION OF ABSTRACT** Unclassified	**20. LIMITATION OF ABSTRACT** UL

NSN 7540-01-280-5500

Standard Form 298 (Rev. 2-89)
Prescribed by ANSI Std. 239-18

THIS PAGE INTENTIONALLY LEFT BLANK

Approved for public release; distribution is unlimited

DIRECT IMAGING OF MINORITY CHARGE CARRIER TRANSPORT IN LUMINESCENT SEMICONDUCTORS

David R. Luber
Captain, United States Marine Corps
B. S., University of Colorado at Boulder, 1999

Submitted in partial fulfillment of the
requirements for the degree of

MASTER OF SCIENCE IN SPACE SYSTEMS OPERATIONS
and
MASTER OF SCIENCE IN APPLIED PHYSICS

from the

NAVAL POSTGRADUATE SCHOOL
September 2005

Author: David R. Luber

Approved by: Nancy M. Haegel
Thesis Advisor

Sherif Michael
Co-Advisor

Rudy Panholzer
Chairman, Department of Space Systems Operations

James H. Luscombe
Chairman, Department of Physics

THIS PAGE INTENTIONALLY LEFT BLANK

ABSTRACT

A quantitative method for extracting minority carrier diffusion and drift lengths is developed and demonstrated in a heavily-doped semiconductor heterostructure. This method advances the high resolution transport imaging technique, yielding key material parameters with a single, non-destructive measurement. This is the first demonstration of an SEM-based, contact-free, non-destructive technique for high-resolution minority carrier lifetime measurement. The measured values are in excellent agreement with theoretical calculations.

The imaging transport technique is also employed to image the nature of the generation region as a function of beam energy, probe current and sample atomic number. These types of images should be useful to allow for experimental verification of resolution limits in CL and EBIC associated with interaction volume effects in bulk materials and can be obtained without additional sample preparation.

Finally, several suggestions for further research are offered, including mapping of radiation damage in solar cells, near-contact E field mapping and studies of low-dimensional structures such as superlattices and quantum wires. These nanoscale structures are poised to usher-in the next revolution in solid-state electronic devices.

THIS PAGE INTENTIONALLY LEFT BLANK

TABLE OF CONTENTS

THIS PAGE LEFT INTENTIONALLY BLANK

LIST OF FIGURES

LIST OF TABLES

THIS PAGE INTENTIONALLY LEFT BLANK

ACKNOWLEDGMENTS

This work was supported by NSF Grant No. DMR – 0203397 and support from a Space and Naval Warfare Systems (SPAWAR) Fellowship.

My appreciation for the daily contributions of LCDR Frank M. Bradley, USN and skillful work on the theoretical model by Mike Talmadge of Fairfield University cannot be overstated. Additionally, the practical and intellectual contributions of Dr. Tom Boone at Hitachi Global Storage in San Jose, CA were invaluable, as was the work performed on multiple samples by Jeff Beeman of Lawrence Berkeley National Laboratory. I also thank my co-advisor, Dr. Sherif Michael.

The work documented in this thesis is a direct testimony to the unwavering patience, sage advice, untiring persistence and keen vision of my mentor and my friend, Dr. Nancy Haegel. Her classroom and her laboratory are rigorous learning environments in which ideas and insights are freely exchanged, discovery is celebrated and hard work is richly rewarded.

I am at once humbled by the relentless support and empowered by the unremitting confidence that my wife, Belinda and my sons, Christopher and Nathan have granted so freely to me during this time. It is all for you.

THIS PAGE INTENTIONALLY LEFT BLANK

I. INTRODUCTION

A. STUDYING TRANSPORT IN SEMICONDUCTORS

A wide range of optoelectronic devices depends upon the generation, recombination and transport of free charge in semiconductor structures. These devices span the electromagnetic spectrum and include, but are not limited to, infrared (IR) detectors, solar cells and ultraviolet (UV) lasers. Therefore, techniques are continually being developed to better understand the spatial variation of luminescence and transport properties of the materials from which these structures are fabricated. Cathodoluminescence (CL) within a scanning electron microscope (SEM) is among the most versatile and widely-used techniques available to the researcher for optoelectronic material characterization [1]. Understanding the interaction of the electron beam (e-beam) with the material is essential in CL for selecting proper operating conditions and interpreting the results. Understanding material transport properties, such as diffusive and drift behavior, is vital in the continuing development of more efficient and radiation-hard solar cells.

In this work, high resolution studies of material transport properties are performed using a new technique developed in our laboratory in 2004 [2]. We call this technique “transport imaging”. This technique is related to conventional CL, wherein the electrons from the SEM e-beam interact with a sample to generate electron-hole (e-h) pairs. Upon radiative recombination, the emitted photons are mapped to the point of e-beam excitation. Unlike conventional CL, however, in transport imaging the e-beam is not scanned and the light collected from the radiative recombination retains the spatial information of its point of origin.

In this thesis, the transport imaging technique has been advanced to a quantitative method for the extraction of minority carrier diffusion and drift lengths. A method for extracting the material transport properties using the slope of the intensity vs. position on a semi-log plot is described and applied to study a

Be modulation-doped p-type AlGaAs/GaAs/AlGaAs heterostructure. In addition, the interaction of the e-beam with a high-Z (bulk GaAs, average Z = 32) and a low-Z (bulk SiC, average Z = 10) material is studied. Finally, parallel-plate and non-standard electric field maps are produced within a heterostructure which demonstrate further potential application of the technique as a high resolution probe of field variations. Feasibility into using such techniques for radiation damage mapping in solar cells is discussed.

B. PURPOSE OF THIS THESIS

The goal is to develop a technique for measurement of key material parameters with a single measurement and $\sim$ 0.5 μm spatial resolution. To that end, the quantitative extraction of transport parameters is developed, transport parameters are successfully extracted from a two dimensional (2D) heterostructure at a range of temperatures from $\sim$ 5K – 300K and the feasibility of directly mapping electric fields in radiation-damaged solar cell materials is demonstrated. Results are presented from the following experiments: interaction volume studies in three-dimensional (3D) bulk materials; diffusion and drift measurements in a 2D heterostructure; preliminary electric field mapping in a 2D heterostructure; transport imaging in a solar cell. These measurements were performed in a SEM with a modified liquid helium-cooled stage and a thermoelectrically-cooled silicon charge coupled device (CCD) camera in the Physics department at the Naval Postgraduate School (NPS).

C. MILITARY RELEVANCE

All space-based remote sensing and communication platforms depend upon the basic physics of charge transport. Solar cells and highly sensitive solid-state photon detectors operate by generating and collecting free charge. The harsh space environment in which these semiconductor materials operate degrades their performance over time by exposing them to harmful radiation. As such, knowledge of charge carrier transport parameters within optoelectronic materials that have been damaged by radiation is essential to the development of

new, radiation-hardened solid-state devices. The experimental technique described in this work could be employed to directly image the effects of radiation damage on transport parameters, significantly aiding in the ongoing development of radiation-hard solar cells and solid-state remote sensing devices.

Understanding material transport parameters is also important in the development of solid-state UV lasers, new, highly efficient terrestrial photovoltaic battery re-chargers and the next generation of spacecraft solar cells capable of increased on-orbit power generation efficiencies and enhanced longevity. Potential cost savings could be realized, as this characterization technique requires minimal or no additional contact processing.

In addition, this high-resolution technique enables the study of spatial inhomogenealities and near-contact electric field behavior. This information is invaluable as semiconductor devices continue to shrink in size. Smaller solid-state devices afford the developer of future systems unique, optimizable combinations of lighter weight, greater efficiency and/or lower cost.

D. THESIS OVERVIEW

Chapter I states the purpose of this thesis, provides an overview of the direct transport imaging technique and describes the relevance to military semiconductor devices. Chapter II provides the reader with the requisite background information to understand the experimental results. This includes a discussion of luminescence in semiconductors, fundamental concepts of charge transport characterization and the photovoltaic effect in solar cells. Chapter III describes the experimental setup, while the studies of the interaction volume are presented in Chapter IV. Transport parameter studies are presented and discussed in Chapter V. Conclusions and suggestions for future research are offered in Chapter VI.

THIS PAGE LEFT INTENTIONALLY BLANK

II. BACKGROUND

A. LUMINESCENCE IN SEMICONDUCTORS

The quantized angular momentum of the electron(s) within a non-radiating atom gives rise to discreet, quantized atomic energy levels that can be specroscopically observed [3]. When many such atoms (e.g. 10^{23}) are brought together within $\sim$ 1 cm^3 to form a crystal, the interatomic interactions give rise to discreet energy bands – distinct allowed and forbidden energy levels [4]. In a semiconductor material the filled energy band, known as the valence band, is separated from the next higher band of allowed energy states, called the conduction band, by a region of forbidden energies known as the band gap. At temperatures above absolute zero, some valence band (VB) electrons are thermally excited into the conduction band (CB), leaving behind an empty electronic state, or a hole. Figure 1 illustrates the interaction of an incident photon of sufficient energy to bridge the band gap $\left(h\upsilon > E_g\right)$ with an electron in the VB, exciting it into the CB, where it is free to contribute to electrical conductivity.

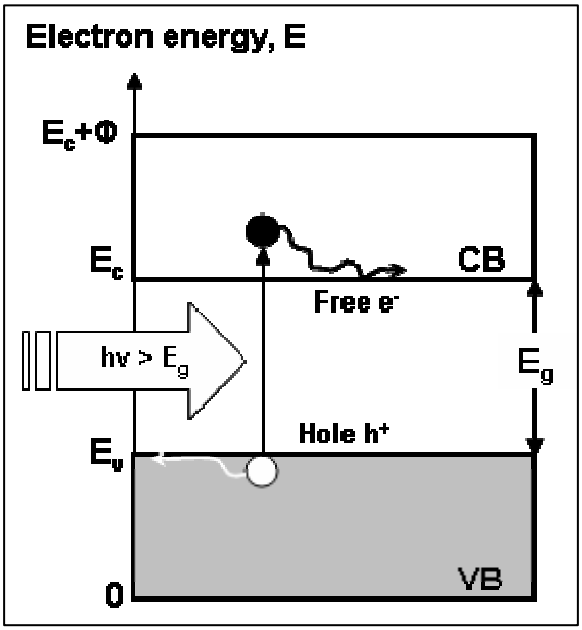

Figure 1 A photon excites an electron from the VB to the CB (adapted from [4]).

In Figure 1, E_v represents the upper edge of the VB, E_c the lower edge of the CB (separated by E_g, the band gap energy), ϕ is the work function (the amount of energy required to completely free the electron from the material), h is Planck's constant and v is the frequency of the incident photon. When sufficient electrons are present in the CB, the material acts as a conductor; when few or no electrons are present in the CB, the material acts as an insulator - hence the name, "semiconductor" for materials where this free carrier concentration can be intentionally controlled.

Conversely, the excited electron can also recombine, moving from the CB to the VB. In an indirect bandgap semiconductor such as silicon, the majority of the recombination is non-radiative, leading to phonon production. In a direct band gap semiconductor such as GaAs, this recombination is often radiative, as the electron emits electromagnetic energy in the form of a photon. One important form of luminescence in semiconductor materials is the emission of band-edge light by an e-h recombination process [5].

B. CARRIER CONCENTRATION

In the laboratory, non-equilibrium e-h pair production is brought about by external excitation in order to study the properties of semiconducting materials. Depending upon the source of the excitation, the resulting luminescence may be categorized as electroluminescence (energy supplied by an electric field), photoluminescence (excitation by photon absorption), chemiluminescence (excitation by chemical reaction), or sonoluminescence (acoustic excitation), among others [1]. In CL, energetic electrons interact with the material, providing the excitation. In this work, the luminescence is created by bombarding the material with the SEM e-beam. Using this technique, it is possible to generate several orders of magnitude more e-h pairs than that produced by PL, which leads to higher signal-to noise ratios and potentially higher resolution experiments due to the short wavelength of the incident electrons.

Let n_{no} be defined as the majority carrier concentration (electron concentration in an n-type semiconductor) and p_{no} be defined as the minority carrier concentration (hole concentration in an n-type semiconductor) in the absence of any external excitation. At thermal equilibrium, the Mass Action Law is obeyed, and

$$n_{no} p_{no} = n_i^2 \tag{1}$$

where n_i is the average intrinsic carrier concentration and is constant for a given temperature. Further, let n_n be the instantaneous majority (electron) carrier concentration and p_n the instantaneous minority (hole) carrier concentration in an n-type semiconductor in the presence of external excitation. The external excitation disturbs the equilibrium, producing excess e-h pairs in equal numbers. Therefore [5],

$$\Delta n_n = n_n - n_{no} = p_n - p_{no} = \Delta p_n \tag{2}$$

and the Mass Action Law is not obeyed. In this n-type material, $n_{no} \approx N_d - N_A$ (the net donor concentration). From Equation 1, $p_{no} = n_i^2 / N_d$, which is significantly less than n_{no}. From Equation 2, it is apparent that even a small change in n_n (such as that by a weak illumination) gives rise to a drastic change in p_n. Therefore, the electrical properties of the semiconductor under external perturbation are often determined by the minority carriers.

C. CONDUCTIVITY, MOBILITY AND LIFETIME

Both electrons in the CB and holes in the VB can contribute to the semiconductor conductivity. From the definition of the current density, in a uniformly doped sample [5],

$$J = env_{de} + epv_{dh} \tag{3}$$

where v_{de} and v_{dh} are the respective electron and hole drift velocities in response to an applied, effectively one-dimensional electric field E_x and

$$v_{de} = \frac{e\tau_e}{m_e^*} E_x ; v_{dh} = \frac{e\tau_h}{m_h^*} E_x . \tag{4}$$

In Equation 4, m_e^* and m_h^* are the effective masses of the electrons and holes, respectively; τ_e and τ_h refer to the mean free time, also known as the electron and hole *lifetime*. The lifetime is a measure of the amount of time a generated charge carrier exists within a material before recombining.

The *mobility* in this context is defined as this proportionality constant between the electric field and the drift velocity:

$$\mu_d = \frac{e\tau}{m^*} . \tag{5}$$

Therefore, in these terms, the conductivity is given by Equation 6:

$$\sigma = en\mu_e + ep\mu_h . \tag{6}$$

For the n-type semiconductor under consideration [4],

$$\sigma = eN_d\mu_e + e\left(\frac{n_i^2}{N_d}\right)\mu_h \approx eN_d\mu_e . \tag{7}$$

Minority carrier lifetime is generally determined by measuring the photoconductivity (or the change in conductivity), as given by Equation 8:

$$\Delta\sigma = e\mu_e\Delta n + e\mu_h\Delta p = e\Delta n(\mu_e + \mu_h) \tag{8}$$

where $\Delta n = \Delta p$ since electrons and holes are generated in pairs. The current density as a result of the illumination is just

$$J_{ph} = \Delta\sigma E. \tag{9}$$

Since $\Delta n = \tau G$, due to the generation rate per unit volume (G), the minority carrier lifetime is [4]

$$\tau = \frac{J_{ph}}{eG(\mu_e + \mu_h)E}. \tag{10}$$

Measurement of lifetime using this approach is limited, however, to the precision to which the generation rate is known.

D. DIFFUSION AND DRIFT

Diffusion in semiconductor materials is the migration of carriers due to a concentration gradient [4]. The diffusion coefficient (D) is a measure of the ease with which a diffusing charge moves through the material and is given by the Einstein relation:

$$D = \frac{kT\mu}{e} \tag{11}$$

where k is Boltzmann's constant, T is the temperature and μ is the mobility. As can be seen in Equation 11, the diffusion coefficient is a function of the mobility, which is also a measure of the ease with which the charge carriers move in the material. As the mobility is given in terms of the effective mass (Equation 5), which differs for the electrons and holes, the diffusion coefficient for electrons also differs from that for holes. The diffusion length $\left(L_{diffusion}\right)$ is a measure of the average length a charge carrier will migrate before it recombines and is given by Equation 12:

$$L_{diffusion} = \sqrt{D\tau} = \left(\frac{(\mu\tau)kT}{e}\right)^{\frac{1}{2}} \tag{12}$$

where all variables are as previously defined.

Drift is the motion of carriers due to an applied bias [4]. The drift length $\left(L_{drift}\right)$ is a measure of the average length a charge carrier will travel due to an applied electric field and is given by Equation 13:

$$L_{drift} = (\mu\tau) E. \tag{13}$$

Note that the $(\mu\tau)$ product appears explicitly in both $\left(L_{diffusion}\right)$ and $\left(L_{drift}\right)$ expressions.

Finally, the total current in a semiconductor material is expressed as

$$J = J_{drift} + J_{diffusion} + J_{displacement} \tag{14}$$

for both electrons and holes. At steady state, $\left(J_{displacement}\right)$ is zero and

$$\begin{aligned} J_e &= e\mu_e nE + eD_e \frac{dn}{dx} \\ J_h &= e\mu_h nE + eD_h \frac{dn}{dx}. \end{aligned} \tag{15}$$

Both the mobility and lifetime must be measured in order to determine a material's characteristic operating diffusion and drift length. A standard technique used for minority carrier lifetime measurements is time-resolved photoluminescence (TRPL) [6]. In TRPL experiments, extremely fast detectors (capable of pico-second resolution) measure the time between excitation by a pulsed laser and e-h recombination by monitoring the time decay of the luminescence. This is a well-established and widely used approach. However, it does not give the complimentary mobility information needed to determine the diffusion or drift length.

Minority carrier mobility has historically been measured using the Haynes-Shockley technique [7]. In this experiment, charge carriers injected at one end of a semiconducting material are moved across the sample under the influence of an electric field. An oscilloscope is used to determine the time delay between the application of the electric field and the arrival of the detected pulse. Knowing the transit time (t) from emitter to collector, the transit distance (x) and the electric field (E), the mobility can be found by Equation 4 ($\mu = \upsilon / E$ and $\upsilon = xt$). This technique requires that the sample be prepared with contacts in order to establish the electric field. A disadvantage to this conventional technique is that

since the mobility measurement is averaged over the entire area between the contacts, material uniformity must be assumed and cannot be easily studied.

E. PHOTOVOLTAIC DEVICES

One very important device that makes direct use of the charge transport properties of semiconductor materials is the solar cell. Solar cells convert incident solar radiation into electrical energy via the absorption of light and the production of mobile charge carriers [4]. These photovoltaic devices are essentially large *p*-*n* junctions that use the internal electric field (E_O) across the depletion region (W) to drift apart the photogenerated e-h pairs [Figure 2].

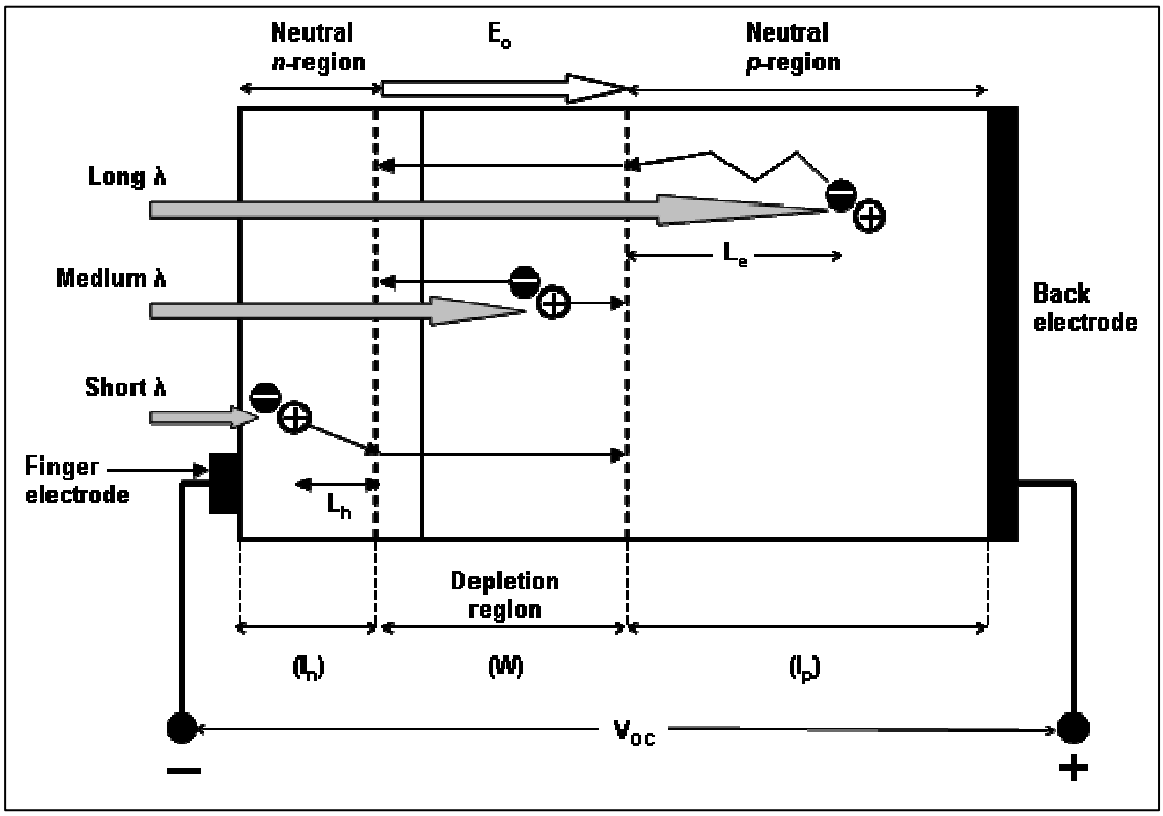

Figure 2 Principle of solar cell operation (adapted from [4]).

An external load (V_{OC}) is applied through which the excess electrons travel away from the *n*-side (l_n), do work, and eventually recombine with the excess holes on the *p*-side (l_p). As will be explained further below, it is usually more

advantageous to use the *n*-on-*p* polarity pictured in Figure 2 versus the possible *p*-on-*n* since in GaAs, for example, the electron (minority carrier) mobility in the base *p*-region is about 20 times higher than that of the hole in the *n*-region [8].

Due to heavy doping, the minority carrier lifetime in the thin *n*-side is very short. Therefore, those e-h pairs that are photogenerated by energetic (short λ) incident photons in this region near the surface or outside the diffusion length (L_h) to the depletion region are lost to recombination. Therefore, the *n*-region is made very thin, typically less than 0.2 μm thick. In fact, the thickness of the *n*-region (l_n) may well be less than the diffusion length (L_h).

Those e-h pairs generated by the medium wavelength (medium λ) photons within the depletion region readily take part in the photovoltaic effect. As depicted in Figure 2, in this region the electrons and holes are promptly separated by the internal electric field.

However, since there is no electric field within the majority of the thick *p*-side (Neutral *p*-region), the e-h pairs that are photogenerated by long wavelength (long λ) photons can only diffuse in this region. Therefore, only those e-h pairs generated within the minority carrier diffusion length (L_e) to the depletion region contribute to the photovoltaic effect; those e-h pairs generated further away are lost to recombination.

The intensity of the light (I) varies from the surface of a semiconductor (x) as [4]

$$I(x) = I_o \exp(-\alpha x) \tag{16}$$

where (I_o) is the intensity of the incident light and (α) is the absorption coefficient. The absorption coefficient is a material property that depends on the incident photon energy or wavelength. For III-V semiconductors such as GaAs and InP, the absorption coefficient rises sharply with increasing wavelength [4]. This is important because the majority of the photon absorption (63%) occurs over a distance $(1/\alpha)$, known as the absorption depth. As the absorption

coefficient is inversely proportional to the wavelength of the incident light, for light near the material band edge, the absorption depth is typically in excess of 100 μm. Consequently, the *p*-region is made correspondingly thick, typically in the 200 – 500 μm range. Minority carrier lifetimes in the micro-second range are not uncommon in solar cell materials, as the higher the minority carrier diffusion length in these thick regions, the greater the solar cell efficiency.

When used in space, the electrical property of solar cells will degrade by particle irradiation from energetic electrons and/or protons [8]. These highly-energetic particles damage the solar cells, creating unwanted non-ionized recombination centers for photogenerated e-h pairs, thereby reducing the output current and voltage. This degradation in performance between the spacecraft beginning-of-life (BOL) and end-of-life (EOL) can be as high as 30% - 40% [9]. Spacecraft designers compensate for this reduction by designing to EOL output power expectations, thereby increasing the solar cell array size. This increase leads to unavoidable inefficiencies in addition to the obvious additional mass that must be lifted to orbit. For example, the extra BOL power can be used for temporary services, but is very often wasted as heat. Therefore, the spacecraft must have design contingencies to remove this unwanted waste heat. Additionally, as the payload requires a constant voltage level throughout a typical mission, power designers must include shunt circuits to accommodate the power degradation over the mission lifetime [8]. These shunts add mass, further increasing the system inefficiency.

From the discussion above, it is apparent that solar cells that exhibit very little power degradation are extremely desirable. Thus, knowledge of the $(\mu\tau)$ product with a high degree of spatial resolution through a simple experimental approach is critical to the solar cell designer.

THIS PAGE LEFT INTENTIONALLY BLANK

III. EXPERIMENTAL APPROACH

A. DIRECT TRANSPORT IMAGING

The direct transport imaging technique presented in this work is a means to experimentally obtain the $(\mu\tau)$ product, and associated minority carrier diffusion length, with a single measurement. This technique directly images the radiative recombination of e-h pairs. It is similar to conventional CL in that electrons interact with the sample to generate e-h pairs. Unlike conventional CL, however, the e-beam is held over a fixed location on the sample and the e-h pair production/radiative recombination processes are brought to a steady state. While much of the light does originate at or very near the point of charge generation, any distribution of the luminescence, whether due to drift, diffusion or interaction volume, is lost in standard CL. In transport imaging, the light collected from the radiative recombination retains the spatial information of its point of origin [2]. By maintaining that information, one can observe the transport of the minority charge. This method can be applied without any additional sample preparation to any luminescent material. In a sample prepared with contacts, the transport imaging method yields the $(\mu\tau)$ product via the minority carrier drift length, provided the applied E field in the material is accurately known.

B. EQUIPMENT

The system consists of a JEOL 840A SEM with an internal optical microscope. A modified, liquid helium-cooled SEM stage (Oxford Instruments) makes it possible to observe luminescence for sample temperatures from ~ 5 – 300K. Figure 3 shows the SEM with the modified stage.

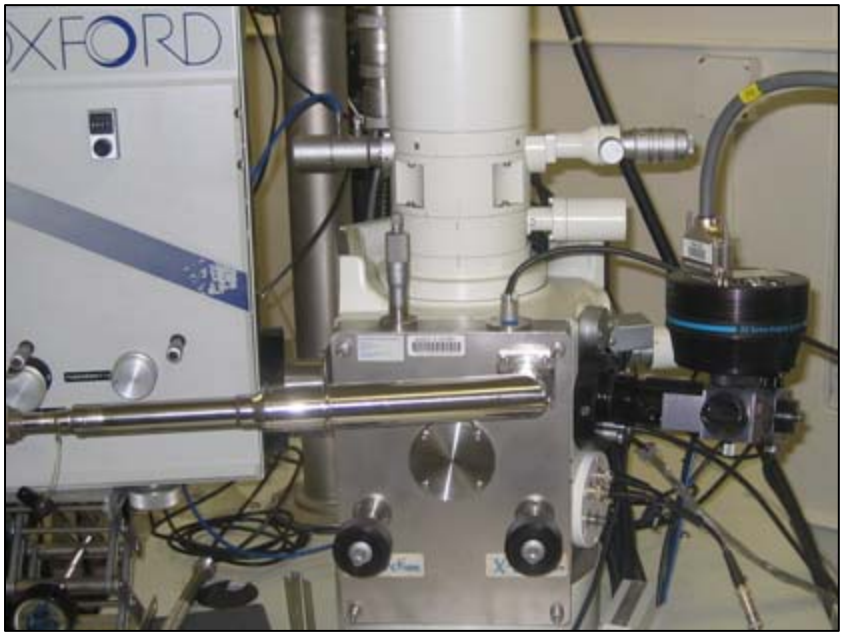

Figure 3 (color) JEOL 840A SEM with modified cold stage.

The optical detector is a thermoelectrically-cooled Apogee silicon charge coupled device (CCD) camera with a 2184 x 1472 pixel array. During operation, the CCD is cooled to about 0^{o} C for noise reduction and collects unfiltered light in the range from ~ 400 to 1100 nm. The pixel size is 8.6 x 8.6 μm and the resolution of the resulting image is ~ 0.4 μm/pixel. This is close to the diffraction limit for the observation of luminescence from room temperature GaAs at ~ 870 nm. The CCD camera is shown in Figure 4; Figure 5 shows a schematic of the full system.

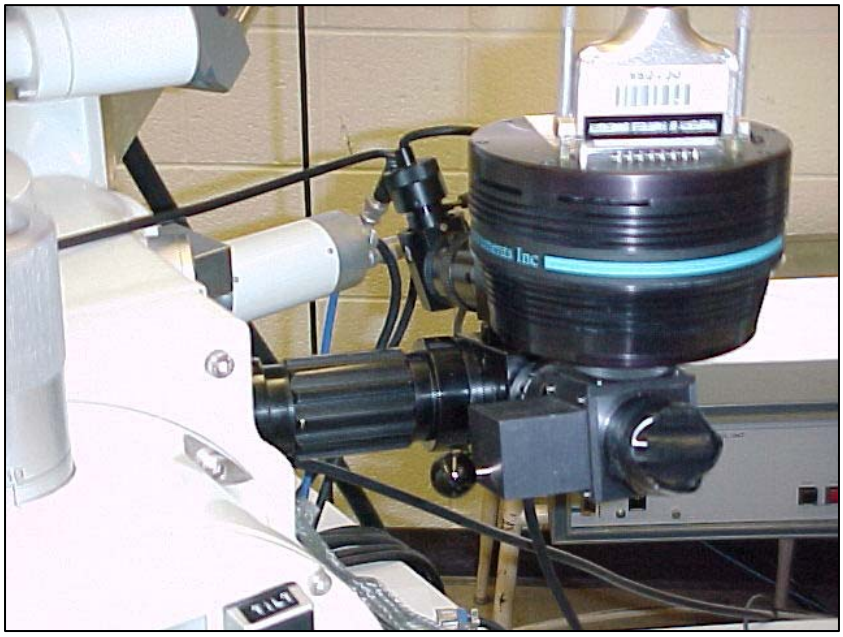

Figure 4 (color) Apogee 2184 x 1472 cooled CCD.

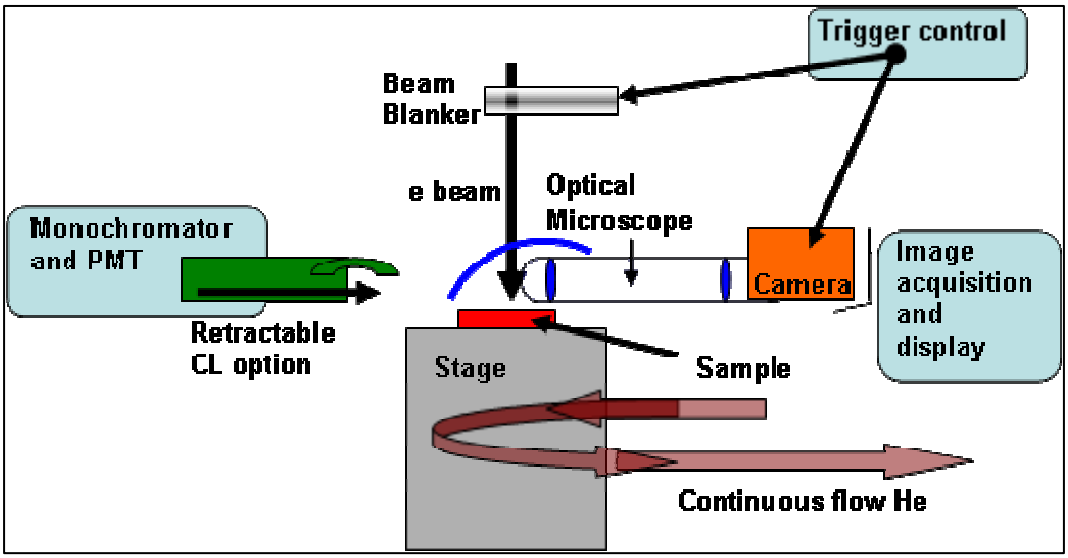

Figure 5 (color) Schematic of transport imaging operating components.

The SEM operating modes used in this work are the picture mode, line mode and spot mode. When in picture mode, the e-beam is rastered over the sample and the luminescence area is recorded by the CCD. Throughout this work, sample features will be depicted using the picture mode, such as the epitaxial mismatching in an 8%-In, GaInAs solar cell shown in Figure 6.

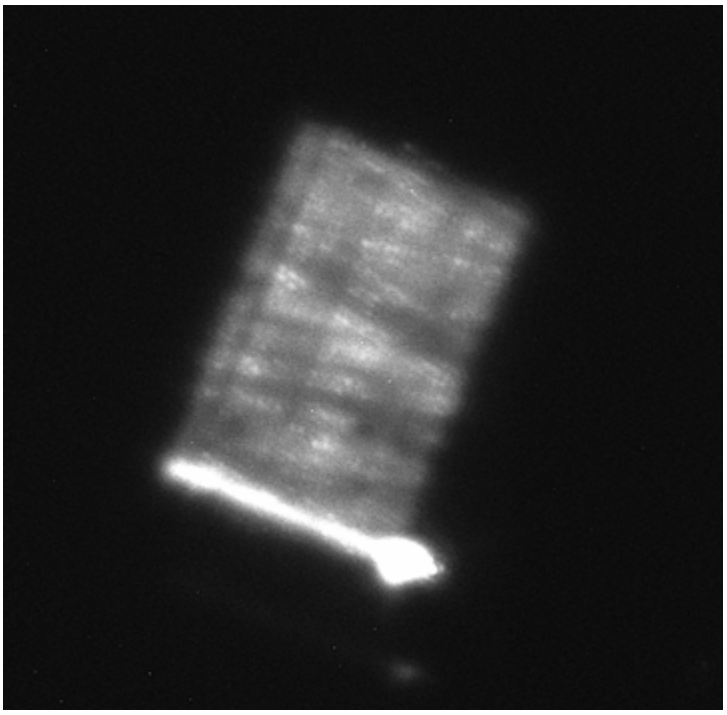

Figure 6 Picture mode example showing the epitaxial mismatching in an 8%-In, GaInAs solar cell (200 μ m x 200 μ m).

The bright line along the bottom edge of the luminescent area with the larger spot at the bottom-right corner is a result of the SEM always scanning the beam longer along one edge of the raster area.

In this work, to visualize dynamic electric field behavior over relatively large areas, the SEM is operated in line mode, during which only a one dimensional (1D) line described above is generated, as shown in Figure 7.

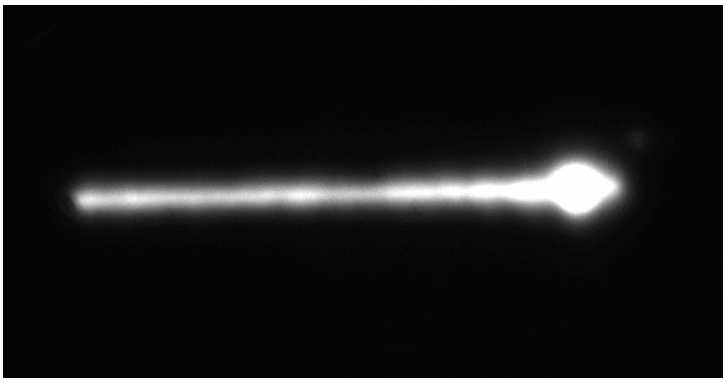

Figure 7 Line mode example in a *p*-type AlGaAs/GaAs/AlGaAs heterostructure (100 μ m x 200 μ m).

Finally, the spot mode is used to generate e-h pairs for diffusive and drift measurements. In this mode, the e-beam is held fixed over a point that is precisely controlled, which allows for local minority charge carrier transport parameter measurements. An example of spot mode operation in a bulk GaAs sample is shown in Figure 8.

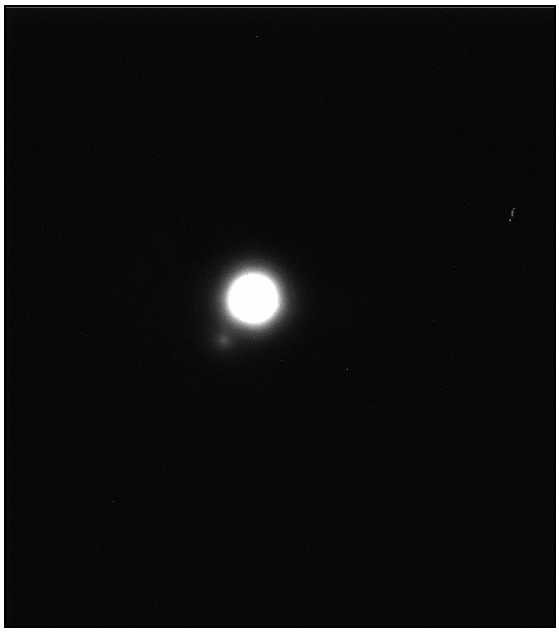

Figure 8 Spot mode example in bulk *n*-type GaAs sample (250 μ m x 285 μ m).

It is important to realize that the observable spot in Figure 8 is not the spot that the e-beam makes when coming into contact with the sample; it is the material luminescence created by the recombination of generated carriers. The spot size of this observed luminescence is much larger than the original e-beam spot size. As the light collected during the transport imaging technique retains the spatial information of its point of origin, it is used to study the material minority carrier properties. Figure 9 shows a 1D line scan of the luminescent spot being taken with the CCD software tool.

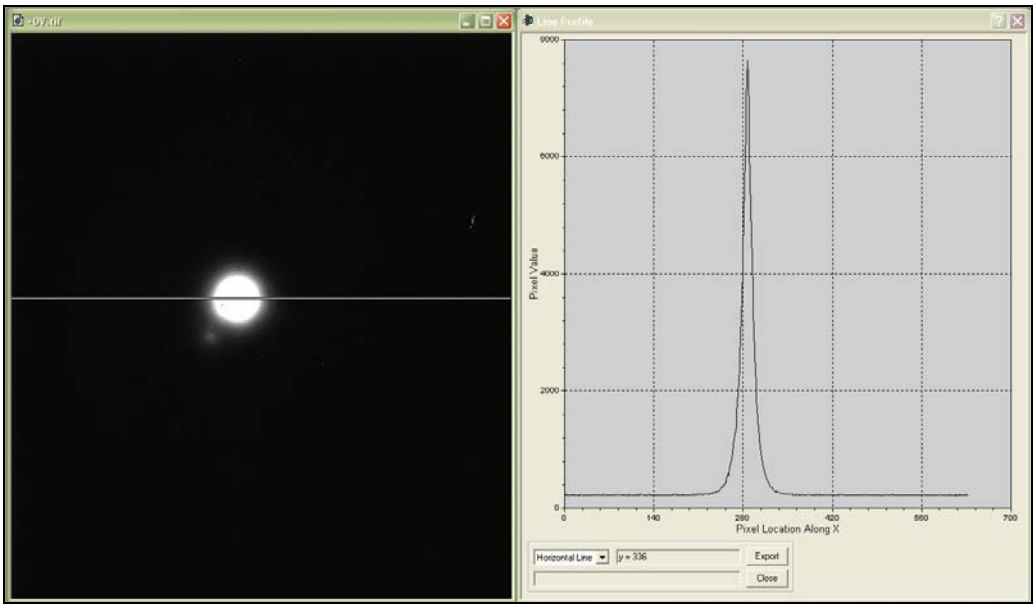

Figure 9 1D line scan taken of luminescent spot (250 μ m x 285 μ m).

When performing transport imaging measurements, the way in which the incident e-beam interacts with the semiconducting material is of natural interest. Therefore, in the next chapter, this technique is initially employed to image the nature of the generation region as a function of beam energy, probe current and sample atomic number in 3D bulk materials.

IV. INTERACTION VOLUME STUDIES

A. PENETRATION DEPTH AND INTERACTION VOLUME

When performing any CL or transport imaging experiments, an e-beam with defined incident energy is used to probe the material. The electrons are negatively charged particles visualized as taking a "random walk" through the electric fields of the sample atoms, depositing their energy in a series of elastic and inelastic scattering events. The *Bethe expression* (Equation 16) describes the mean rate of energy (E) loss per unit of distance (S) traveled, due to an inelastic scattering event:

$$\frac{dE}{dS} = -2\pi \cdot e^4 \cdot N_A \cdot \frac{\rho Z}{E_i A} \cdot \ln\left(\frac{1.166 E_i}{J}\right)\left(\frac{keV}{cm}\right) \tag{16}$$

where e is the electronic charge in Coulombs, N_A is Avogadro's number, ρ is the density in g/cc, *A* is the atomic weight in g/mole, E_i is the electron energy in keV at any point in the spectrum and *J* is the mean ionization potential [1]. However, the more interesting parameter in application is the total depth (perpendicular to the sample surface) over which the energy is dissipated. Integrating the Bethe expression over the energy range from the incident value to a low threshold value gives an estimate of the Bethe range, or the total distance the electron can travel while undergoing randomizing elastic and inelastic scattering events. The *penetration depth*, according to a commonly used expression by Kayana and Okayama, is given by:

$$R_e = (0.0276 A / \rho Z^{0.889}) E_b^{1.67} (\mu m) \tag{17}$$

where E_b is the electron energy in keV, A is the atomic weight in g/mol and ρ is the material density in g/cc [1, 10]. This depth, together with the lateral extent (parallel to the sample surface) over which the energy is deposited into the sample, define the *interaction volume.* One highly-energetic (e.g. 20 keV)

incident electron can lead to the generation of thousands of e-h pairs within the interaction volume, depending on the semiconductor bandgap energy.

B. PREVIOUS STUDIES OF THE INTERACTION VOLUME

The shape of the interaction volume depends on the incident energy, the angle of the electron beam and the atomic composition of the sample [11]. Most theoretical studies of the interaction volume involve Monte Carlo calculations using different functions to represent the penetration depth and the lateral dependence of the energy dissipation [12].

Goldstein et. al., reviews the findings of early experimental studies performed by Everhart et. al., of the interaction of an electron beam normal to the surface of the plastic material polymethylmetacrylate (PMMA), a material used as an electron-beam resist for patterning [11, 13]. In this experiment, a series of successively longer chemical etchings for samples exposed to constant electron dose reveal the contours of e-beam energy deposition within the interaction volume. The interaction volume for this low-density, low-Z material was found to exhibit a distinct pear shape for the lowest energy deposition contours as shown in Figure 10.

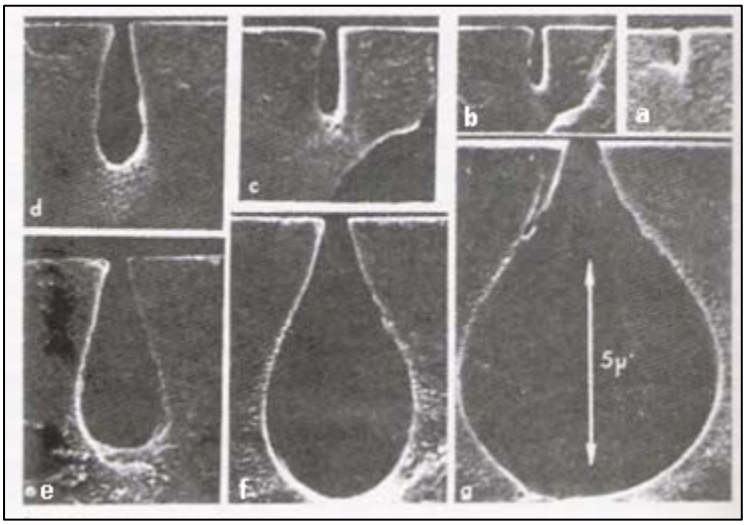

Figure 10 PMMA etching experiment: (a) corresponds to the shortest etching time, (g) to the longest, revealing the distinctive pear shape [11].

This result is understood theoretically in terms of the effects of elastic and inelastic scattering of the primary electrons. The elastic scattering interactions with the nuclei of the material lead to large-angle deviations of the electron path with very little energy loss, thereby causing a lateral spreading of the interaction volume. The inelastic scattering events lead to small-angle deviations and correspondingly large energy depositions into the sample [11]. Since elastic scattering is relatively less probable ($\sim Z^2$) in the low-Z PMMA material, the electrons travel deeper into the sample before spreading, in good agreement with the Monte Carlo calculations.

Although the PMMA etching experiment provides representative results that are important for low-Z materials, there are no intermediate or high-Z materials for which a similar approach can reveal the interaction volume. Therefore, Monte Carlo simulations of the electron trajectories have been the primary means to explore these cases.

A recent review of local probe techniques for luminescent studies also discusses current understanding of the interaction volume and surveys related work [6]. Efforts to probe the lateral extent of the generation volume have been done with both CL and electron beam induced current (EBIC) [6, 14, 15, 16]. In one set of experiments, the depth and lateral generation profiles in $Al_{0.4}Ga_{0.6}As$ have been experimentally probed using CL measurements in samples prepared with a multiple-quantum-well (MQW) structure as an internal detector [14, 15]. The wavelength signature associated with the radiative recombination from the quantum well was used to isolate the generation within a 50 Å region, with the barrier layers preventing diffusion into or out of the well. The interaction volume was probed by varying the beam position in two different orientations. Good agreement with the Monte Carlo simulations was found, once accurate analytic expressions were developed for the depth-dose and lateral dependence functions. This method has the obvious limitation that it is applicable only to materials that support MQW growth, and a sample must be uniquely prepared.

C. INTERACTION REGION IMAGING

The direct transport imaging technique is employed to study the interaction volume in a high-Z (GaAs, average Z = 32) and a low-Z (SiC, average Z = 10) material at room temperature with the e-beam at normal incidence to the sample. No special sample preparation is required, as long as the material has a luminescent signature of interest.

Figure 11 shows the image obtained with a 1 nA, 30 keV e-beam incident on a 400 μm-thick bulk *n*-type Si-doped GaAs sample with a donor concentration of $\sim$ 6 x 10^{17} cm^{-3}.

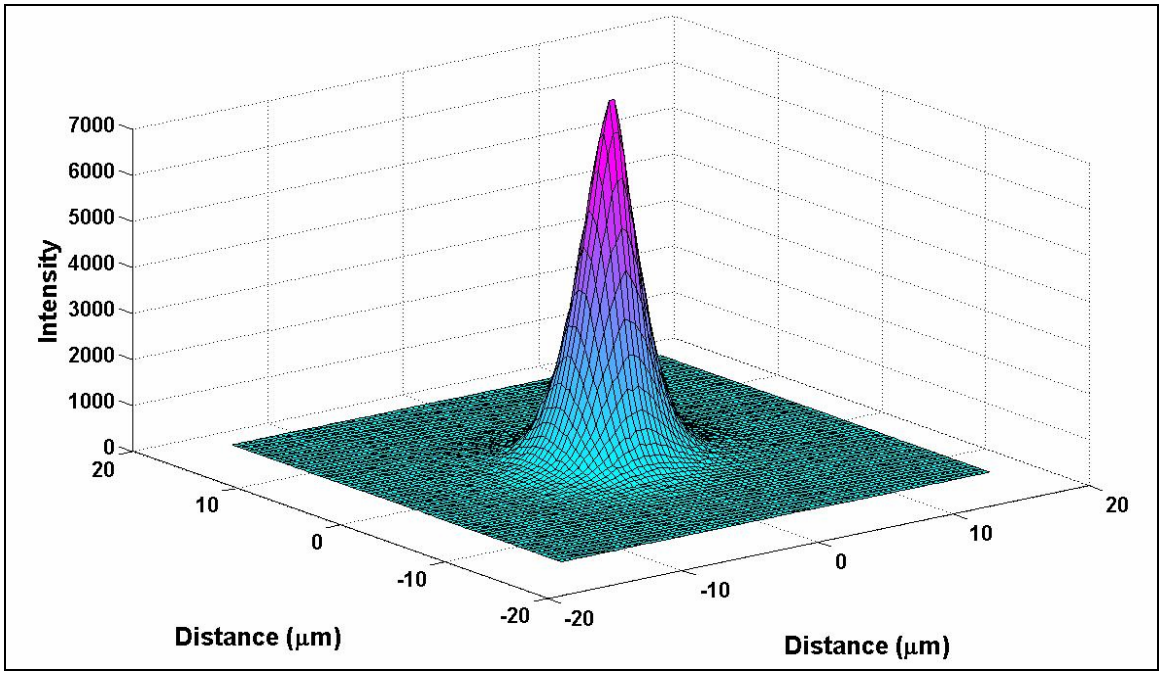

Figure 11 (color) Luminescence image from GaAs under spot mode excitation with e-beam parameters of 30 keV and 1 nA. Luminescence intensity is plotted on the z axis.

Figure 12 shows the image obtained from a 265 μm-thick bulk, doped *n*-type SiC (6H crystal) with a 6 x 10^{-8} A, 30 keV incident e-beam.

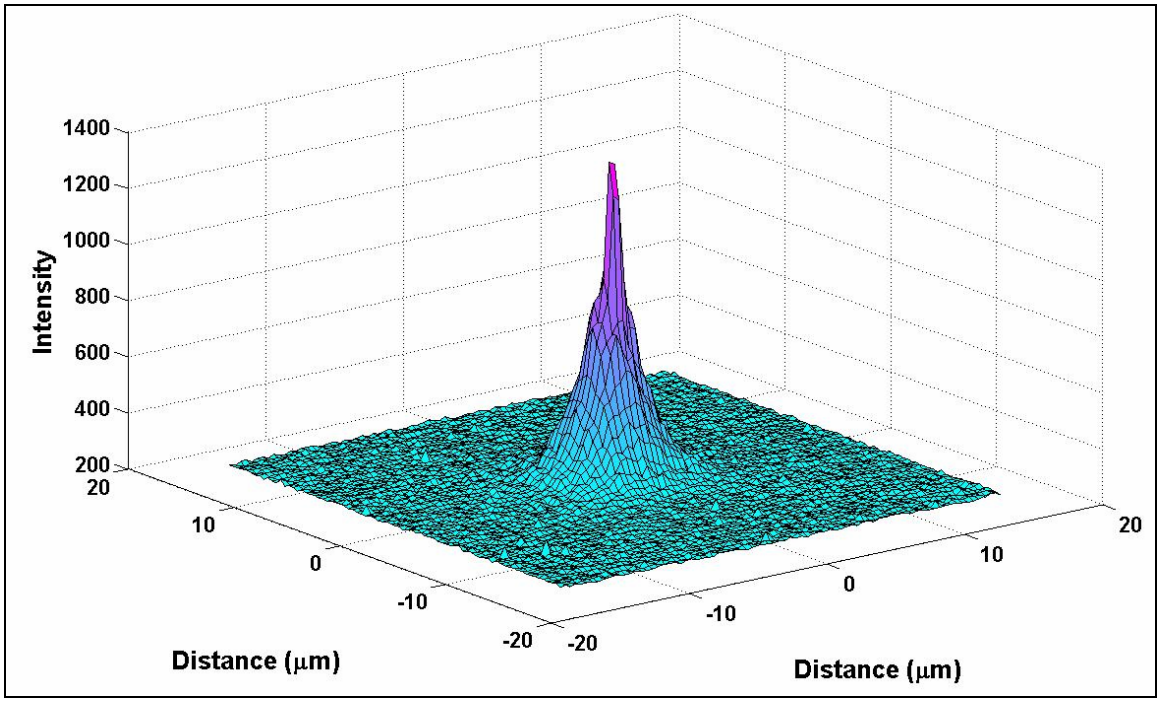

Figure 12 (color) Luminescence image from SiC under spot mode excitation with e-beam parameters of 30 keV and 6 x 10^{-8}A.

The intensity of the light is again plotted in the z direction, with x and y mapped to pixels on the CCD. Because a 2D projection is observed, the term *interaction region* is defined as the projected area of the interaction volume.

In both the GaAs and SiC cases, the thickness of both samples is much greater than the maximum penetration of the e-beam. Therefore, these results are in the 3D limit for carrier diffusion from the initial generation volume. This leads to a concentration distribution

$$n(r) \sim (1/r) \times \exp\left(-r / L_{diff}\right) \tag{18}$$

for carriers generated at a point source, where L_{diff} is the diffusion length [6]. Even for large variations in diffusion lengths, this expression is only weakly dependant on L_{diff}. In standard CL, this effect has been shown to allow for higher resolution than might otherwise be expected in materials with long

diffusion lengths [12]. This is not true in 2D (e.g. epitaxial or thin films with thickness comparable to the diffusion length), since the diffusion dependence in that case is

$$K_o\left(r / L_{diff}\right) \tag{19}$$

where K_o is the zeroth order modified Bessel function of the second kind, and is much more sensitive to variations in L_{diff}. Figure 13 is a representation of the generation volume in a thin (2D) versus a thick (3D) sample.

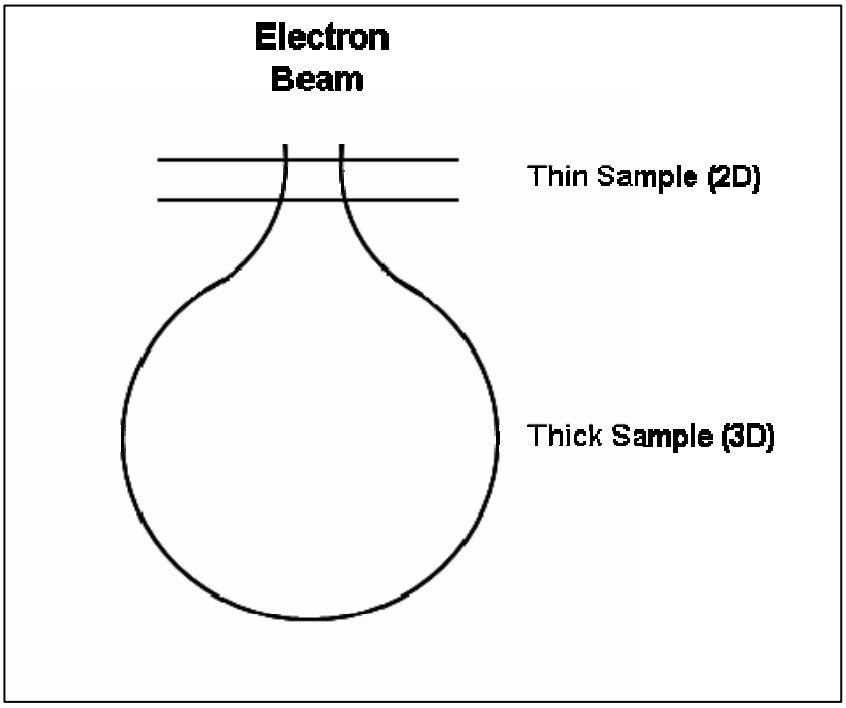

Figure 13 Generation Volume, 2D and 3D sample.

In addition, in this experiment both materials have diffusion lengths that are much shorter $\left(L_{diff} < 1\,\mu m\right)$ than the generation region of interest due to the doping concentrations. Therefore, due to both the small values in L_{diff} these materials and the 3D nature of the diffusion, these images reflect the interaction volume, with minimal effect of the diffusion of the minority charge carriers.

Information can then be directly obtained about both the 2D extent of the region and the variations of minority carrier distributions within that region.

There are three primary mechanisms that would cause recombination and luminescence at points removed from the original generation volume: diffusion of carriers, carrier drift and photon recycling associated with recombination and subsequent reabsorption and emission. In this work, diffusion is minimal, as previously discussed and the experiments are done in the absence of applied field. Photon recycling may make some contribution to the spreading of the image, however, results as a function of probe current will show that this effect is also negligible on this scale. To the extent that it does occur, however, it is included, which is appropriate, given that it will also be a factor to any CL and EBIC measurements under similar conditions. The images allow direct visualization of the response to spot excitation.

Figure 14 shows one dimensional line scans from GaAs interaction region images (e.g. Figure 11), normalized to the maximum intensity point, as a function of incident beam energy. Scans are from images taken from 5 to 30 keV, in 5 keV steps, with a fixed probe current of 1 nA.

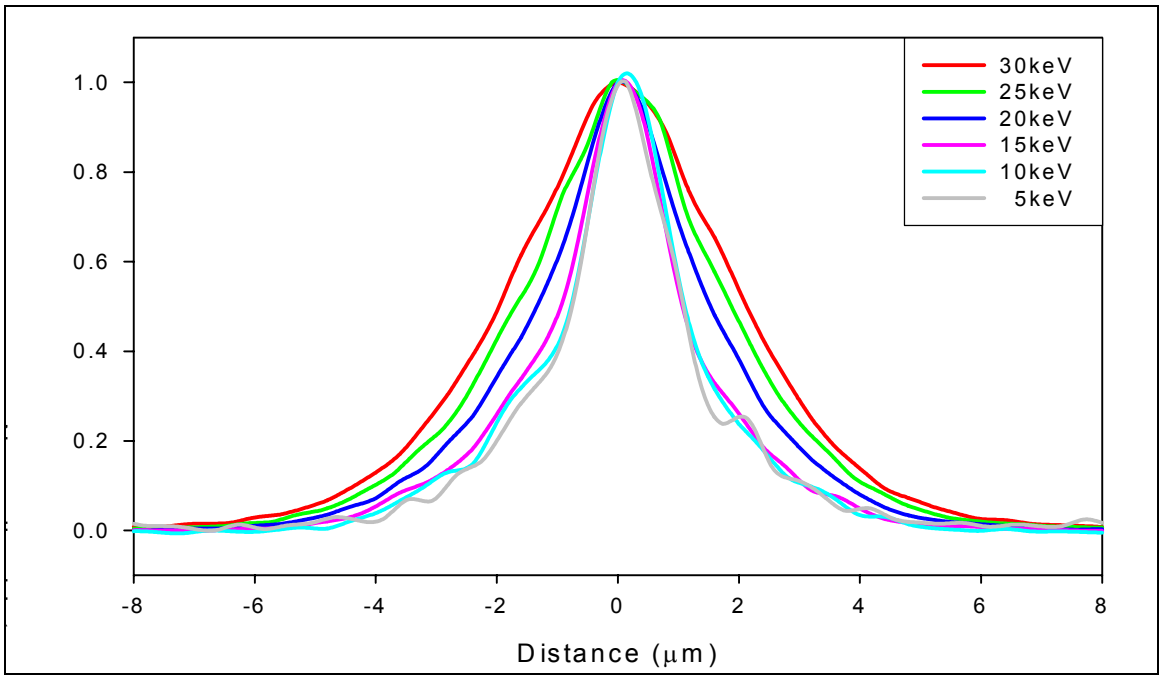

Figure 14 (color) Intensity distribution as a function of position for GaAs with probe current of 1 nA and beam energies from 5 to 30 keV.

As expected, an increase in the interaction region is observed with increasing voltage, consistent with previous work [6, 8, 11, 12]. The full-width at half-max (FWHM) increases from approximately 2 μm to 4 μm as the beam energy increases from 5 keV to 30 keV in the GaAs sample. A similar trend was observed for the SiC sample, using a 6 x 10^{-8} A beam, as shown in Figure 15.

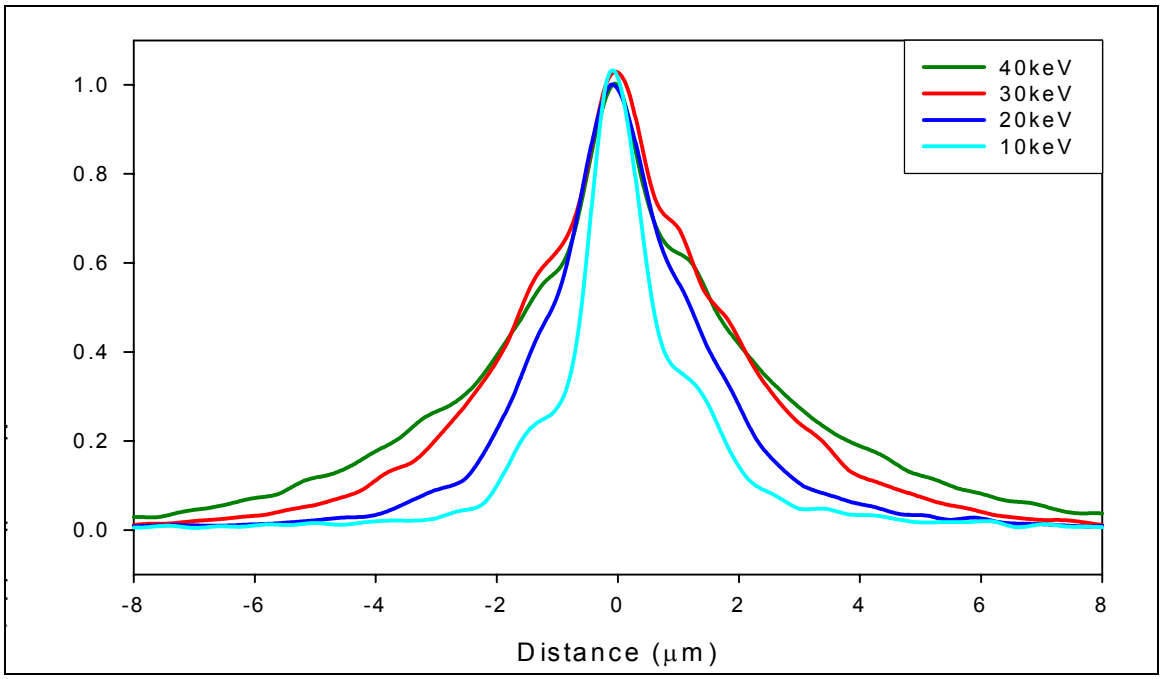

Figure 15 (color) Intensity distribution as a function of position for SiC with probe current of 6 x 10^{-8}A and beam energies from 10 to 40 keV.

The influence of the e-beam probe current on the lateral distribution and local generation volume shape has also been studied in both samples. The results from the SiC sample, using a 30 keV e-beam and varying the probe current over three orders of magnitude, are shown in Figure 16.

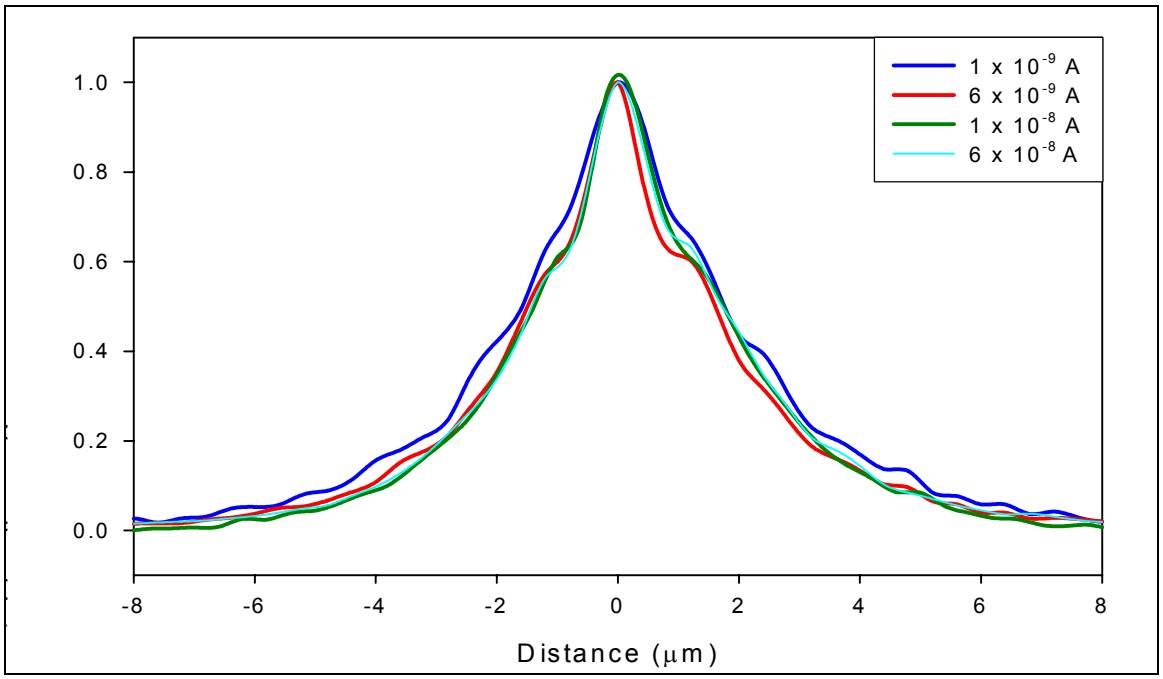

Figure 16 (color) Intensity distribution as a function of position for SiC with beam energy of 30 keV and probe currents of 1 nA, 6 nA, 1 x 10^{-8} A and 6 x 10^{-8} A.

One sees that, for this beam energy, the lateral extent of the generation volume is only slightly affected by the changing probe current. This is expected, since the beam diameter at the surface is much less than the interaction region width. For a 30 keV e-beam, the spot size at 3 x 10^{-10} A is expected to be approximately 60 nm; a 1 x 10^{-8} A beam yields a spot size of ~ 150 nm [11]. This local variation in beam diameter is observed to have only a minor effect on the extent of the interaction region which is determined primarily by incident electron energy. Similar results were found for the GaAs sample.

The insensitivity of the measured luminescence profile to probe current also demonstrates that the measurements are made in the “low excitation” limit. As a result, they image minority carrier recombination in an approximately constant majority carrier distribution. The ability to operate in this limit over a wide range of excitation is due to the heavily doped nature of the samples. Drift experiments have also previously demonstrated that we observe predominately

minority carrier recombination for a range of doping levels, based on the direction of drift in a given applied field [2].

The generation region as a function of material parameters is considered by comparing the generation region for SiC and GaAs at a fixed beam energy of 30 keV and a probe current of 1 nA [Figure 17]. The images from which these line scans were extracted were taken so that all beam conditions (filament current, emission current, aperture) were unchanged. One sees significant variations in the luminescence within the generation region due to the change in material properties.

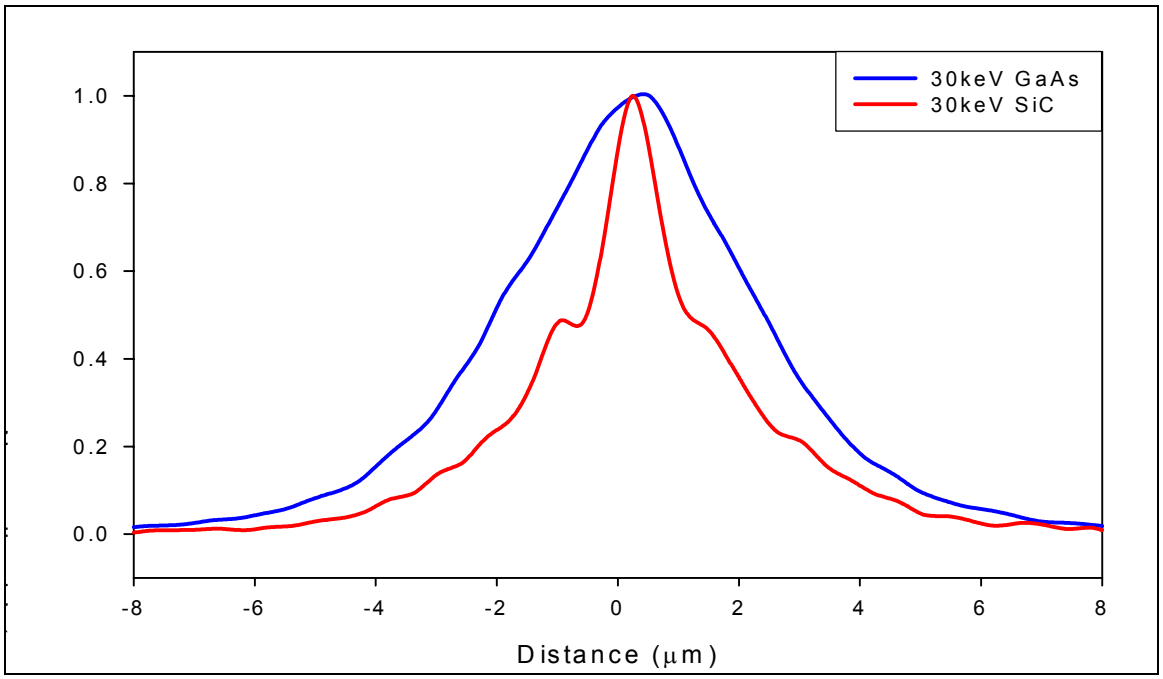

Figure 17 (color) Intensity distribution for GaAs and SiC; 30keV, 1 nA.

The Monte Carlo electron trajectory simulations reviewed by Goldstein et. al. show a significant change in interaction volume shape as a function of atomic number. In that analysis, a change from the characteristic pear shape in low-atomic-number materials to a more nearly hemispherical shape for high-atomic-number materials was reported [11]. The generation region of the SiC plot in Figure 17 is consistent with a deeply-penetrating pear shaped interaction volume within the low-Z material. The shape of the GaAs plot is well-described by a

more hemispherical interaction volume truncated by the plane of the surface. However, we do not observe an increase in linear extent for the low Z material, as might be expected from the Monte Carlo calculations. These experiments consistently show a narrower luminescence distribution for the low-Z than for that of the high-Z material.

Finally, the 3D images of the luminescence distribution in the SiC sample for two additional cases are compared. Figure 18 shows the image with incident electrons at 10 keV and a beam current of 6 x 10^{-8} A. Figure 19 shows similar results for electron energies of 40 keV.

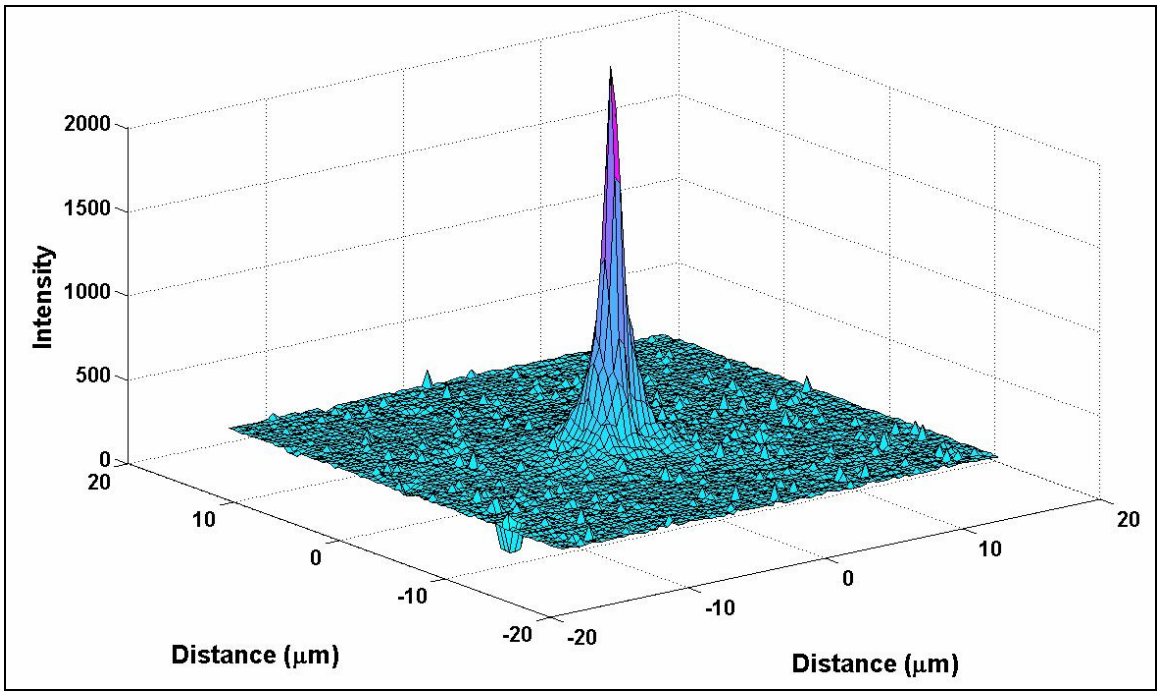

Figure 18 (color) Luminescence image from SiC under spot mode excitation with e beam of 10 keV and 6 x 10^{-8}A.

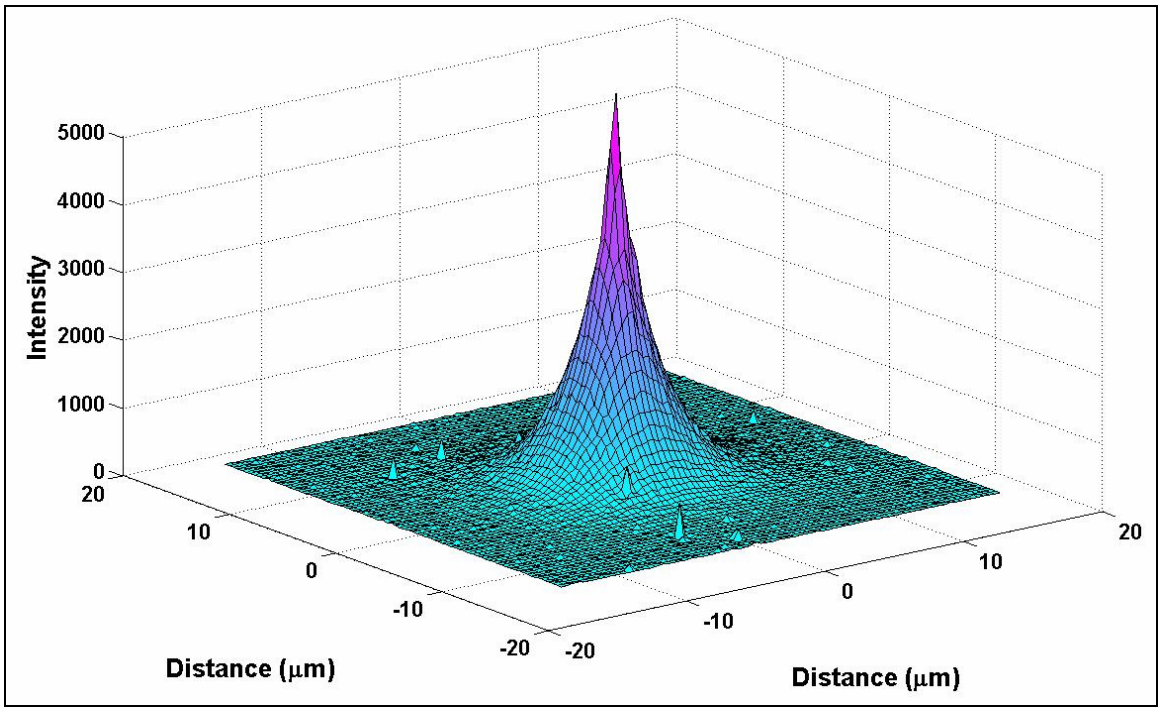

Figure 19 (color) Luminescence image from SiC under spot mode excitation with e beam of 40 keV and 6 x 10^{-8}A.

One observes both the narrow internal distribution associated with the interaction in the low-Z material and the broadening of the interaction region with increasing incident beam energy.

As is evidenced in this work, transport imaging is not ideal for measuring L_{diff} in bulk samples, due to the generation volume. Application of this technique to effectively 3D samples requires that $L_{diff} \gg$ generation dimension to overcome the insensitivity of the carrier concentration to the minority carrier diffusion length. The lower the dimensionality of the material being considered, the greater the sensitivity this approach is to L_{diff}. In the following chapter, a quantitative method of extracting the minority carrier diffusion and drift lengths is described and used to make optical measurements in a 2D heterostructure.

THIS PAGE LEFT INTENTIONALLY BLANK

V. TRANSPORT PARAMETER STUDIES

A. BOONE SAMPLE 9

The transport imaging technique is applied to quantitatively extract the $(\mu\tau)$ product and minority charge carrier diffusion length from a 1000 Å-thick (effectively 2D) active GaAs layer of an AlGaAs/GaAs/AlGaAs heterostructure, modulation-doped p-type with Be at ~ 5 x 10^{18} acceptors/cm^3, herein referred to as "Boone Sample 9". This sample was provided by Dr. Tom Boone from the Hitachi Corp. in San Jose, CA, whose TRPL measurements indicate that the minority carrier (free electron) lifetime for this sample is 4320 pico-seconds. Mesa structures were etched into the sample and non-alloyed Ti:Au electrical contacts were deposited and lithographically defined on top of the mesas [17]. Quantitatively extracting the $(\mu\tau)$ product and knowing the lifetime of the minority carriers, an estimate can be made of their mobility and compared to theoretical minority carrier mobility calculations in heavily doped p-type GaAs based upon quantum calculations by Bennett [18] as outlined below.

1. Imaging Drift

In samples prepared with electrical contacts, such as Boone Sample 9, a voltage bias is applied across the contacts to establish an E field as represented in Figure 20. Application of the E field causes the charge carriers to drift. The minority electron drift "tails" are in the direction of the positive contact and radiatively re-combine in a p-type material, as modeled in Figure 21.

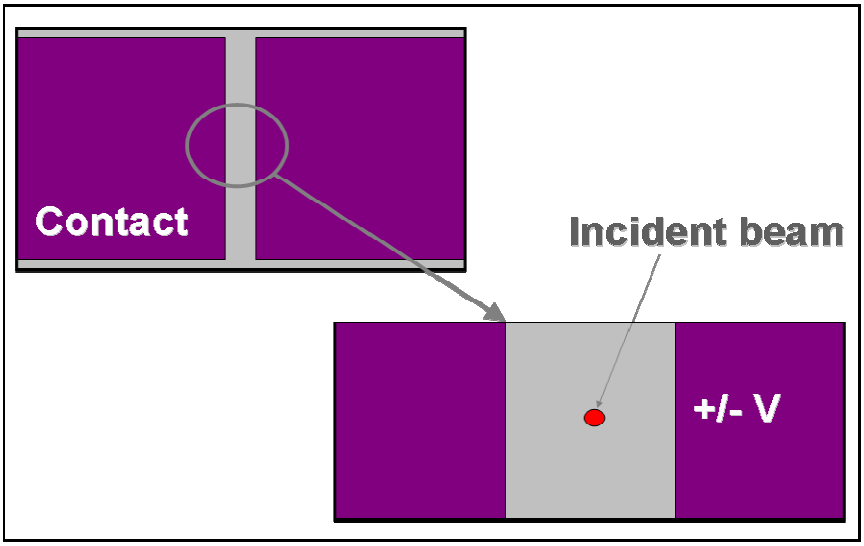

Figure 20 (color) Representation of a sample prepared with contacts (purple areas). The gray area represents the sample.

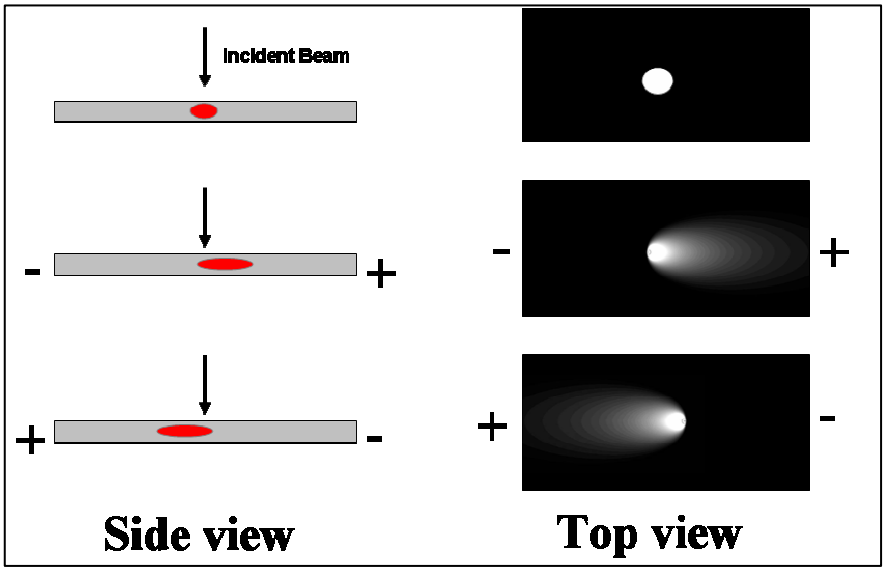

Figure 21 Drifting minority electrons modeled in a p-type material.

For an n-type material, the minority carriers are holes and the drift tails are observed in the direction of the negative contact upon radiative recombination [2]. Since band-edge light is imaged, filters are used in the optical train to remove any unwanted light from layers other than the active layer of interest. In this work, a 750 nm long-pass filter is used just before the CCD camera shutter to remove any extra luminescence from the AlGaAs barrier layers. As the

generation/radiative recombination processes are at steady state while imaging transport, the CCD exposure time is adjusted to provide adequate intensity for quantitative measurements.

2. Quantitative $(\mu\tau)$ Extraction via Slope-matching

A room temperature transport imaging measurement was made using an e-beam accelerating voltage of 20 keV and current of 3 x 10^{-10} A in Boone Sample 9. Figure 22 shows pseudo-color images of the interaction region and the diffusion and drift tails as a function of accelerating voltage.

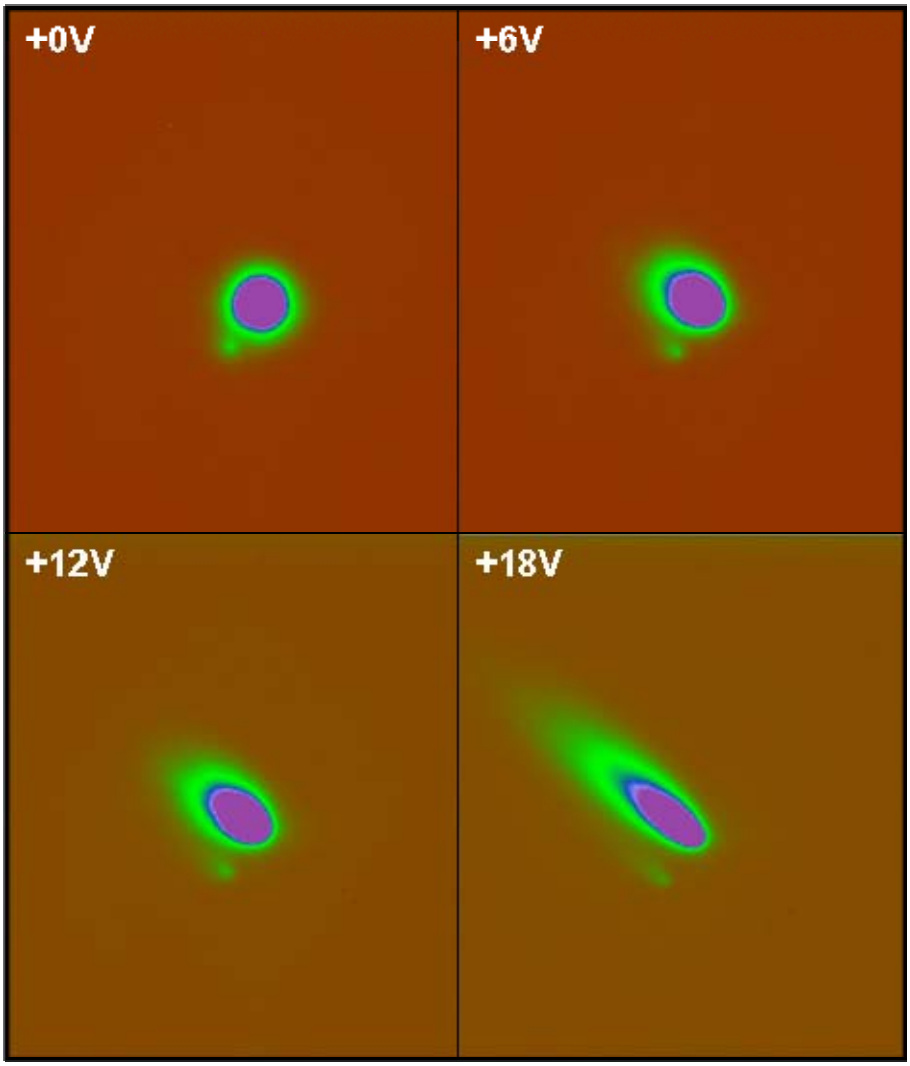

Figure 22 (color) Boone Sample 9; 20 keV, 3 x 10^{-10}A e-beam. Each image is ~ 200 μm x 220 μm (full area).

For this p-type material, the minority charge carriers are electrons drifting toward the positive-biased contact in the direction depicted in the figure. Note the small luminescent spot just beneath the interaction region. This spot is believed to be a reflection internal to our optical microscope and is seen in all images of this type. It can be subtracted from the picture but is routinely ignored as it has no bearing on the quantitative analysis that follows.

Figure 23 shows the 1D line scans of the linear normalized intensity curves as a function of linear position in the direction of the diffusive and drift tails for increasing E-field; Figure 24 shows the same data on a semi-log plot (linear in X, logarithmic in Y).

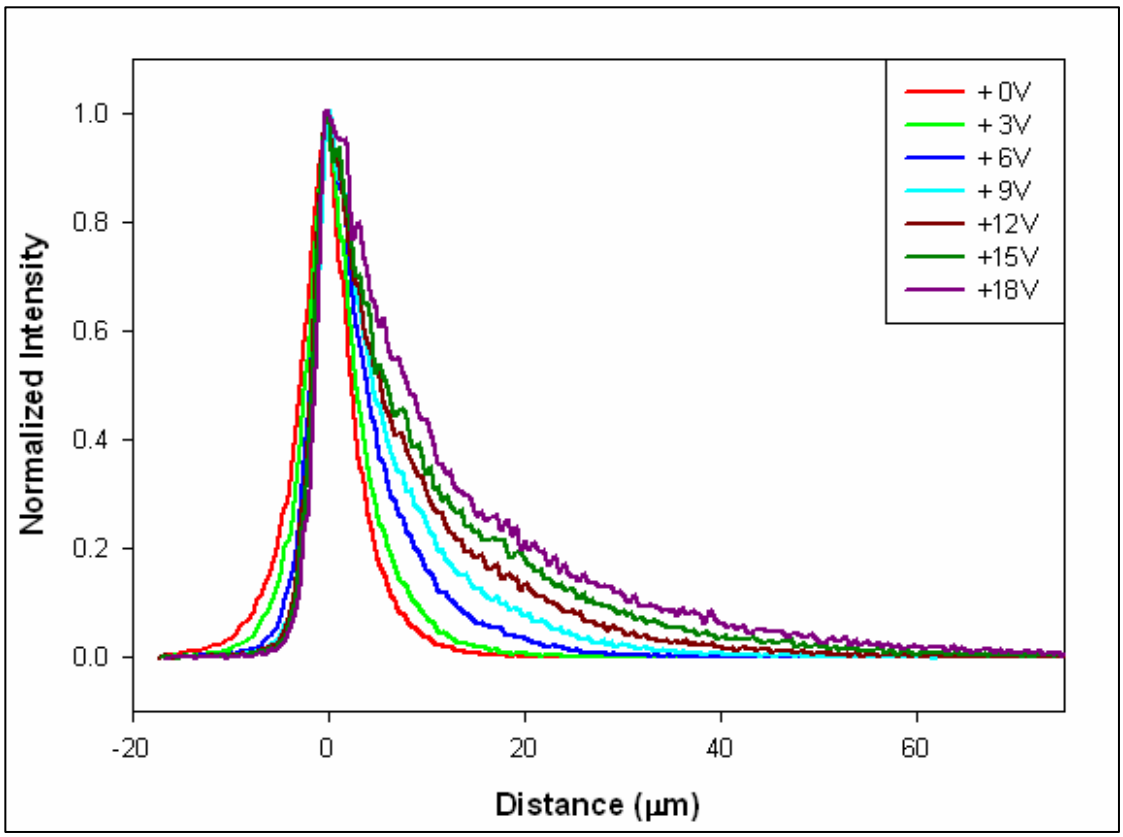

Figure 23 **(color) Boone Sample 9 Intensity vs. Distance (Linear) taken through the center of the incident spot, in the direction of the minority carrier drift tails, using a 20keV, 3 x 10^{-10}A e-beam.**

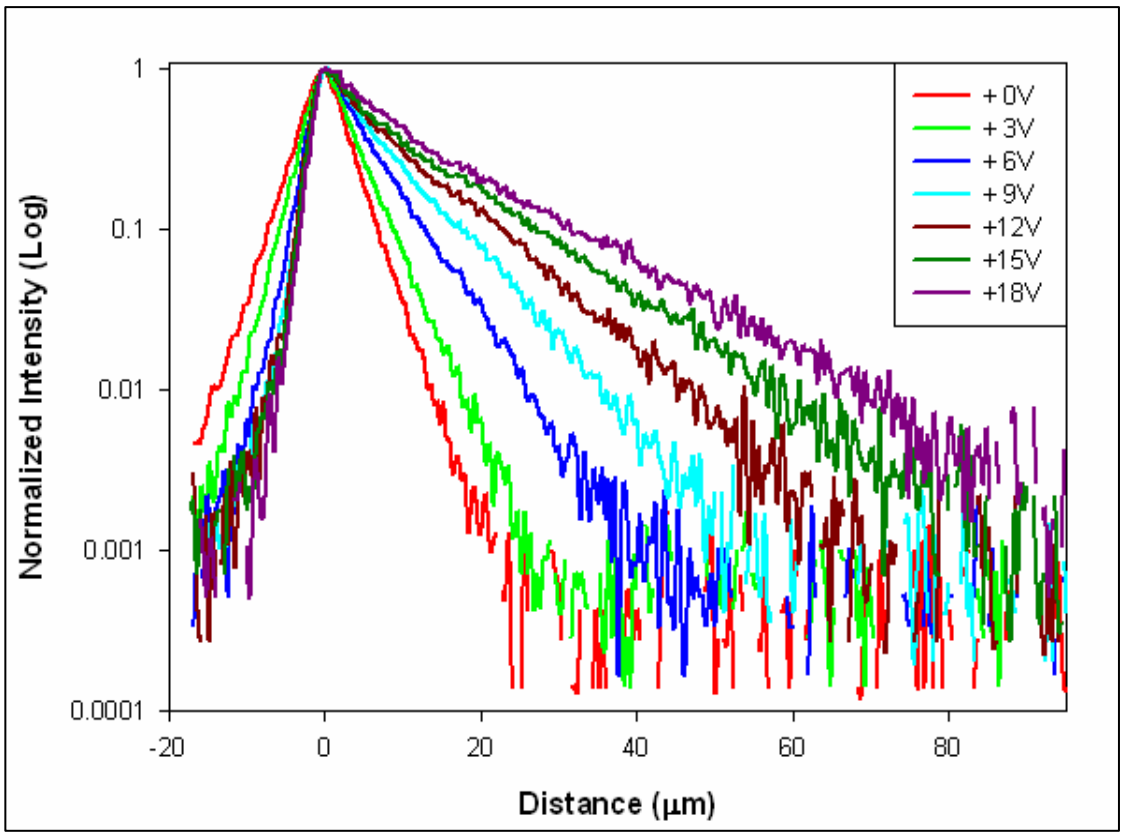

Figure 24 (color) Boone Sample 9 Intensity vs. Distance (Semi-log), as in Figure 23, using a 20keV, 3 x 10^{-10}A e-beam (Linear in X, Log in Y).

On the semi-log plot depicted in Figure 24, the drift tails appear to be nearly linear, suggesting a simple negative exponential governing function. Boaz shows that, in the limit of large (x), the Bessel function $\left(K_p(x)\right)$ can be approximated by a simple negative exponential [19]:

$$K_p(x) \approx e^{-x} + O\left(\frac{e^{-x}}{x}\right) \tag{20}$$

The symbol $O\left(\frac{e^{-x}}{x}\right)$ stands for terms of the order of x^n or less and means that the error in the given approximation is less than a constant times x^n. The theoretical model that describes minority carrier distribution from a point source in the presence of diffusion and drift, given in Equation (21):

$$Intensity = \frac{1}{2\pi} \cdot e^{\frac{S \cdot x}{2 \cdot L^2}} \cdot K_0 \cdot \left[\frac{\left(\sqrt{S^2 + 4L^2}\right) \cdot \left(\sqrt{x^2 + y^2}\right)}{2L^2} \right] \tag{21}$$

In the model, S is the Drift Length (Equation (13)) and L is the Diffusion Length (Equation (12)). So, out in the drift tails where the large (x) approximation is assumed, the Point Generation model becomes:

$$Intensity \approx e^{\frac{+S \cdot x}{2 \cdot L^2}} \cdot e^{\frac{-\sqrt{S^2 + 4 \cdot L^2}}{2 \cdot L^2} x} = e^{C \cdot x} \tag{22}$$

where C is the slope. Solving for C:

$$C = \frac{S}{2L^2} + \frac{-\sqrt{S^2 + 4L^2}}{2L^2} = \frac{S - \sqrt{S^2 + 4L^2}}{2L^2} \tag{23}$$

Now, let $S = nL$ (so $n = 0$ corresponds to purely diffusive behavior and large (n) corresponds to dominant drift behavior):

$$C = \frac{nL - \sqrt{(nL)^2 + 4L^2}}{2L^2} = \frac{nL - L\sqrt{n^2 + 4}}{2L^2} = \frac{n - \sqrt{n^2 + 4}}{2L_{diff}}. \tag{24}$$

As can be seen for the above equation for C, for purely diffusive behavior $(n = 0)$, the slope provides the diffusion length $\left(L_{diff}\right)$, as:

$$C = \frac{-1}{L_{diff}} \tag{25}$$

And with increasing (n), corresponding to increasing E field, the slope decreases to the limit where $C = 0$ for very large (n).

Figure 25 shows that linear regression curves fit to the experimental data do, indeed follow the general trend predicted above. Note that the linear fit is applied in the tail (less than 10%) of the distribution.

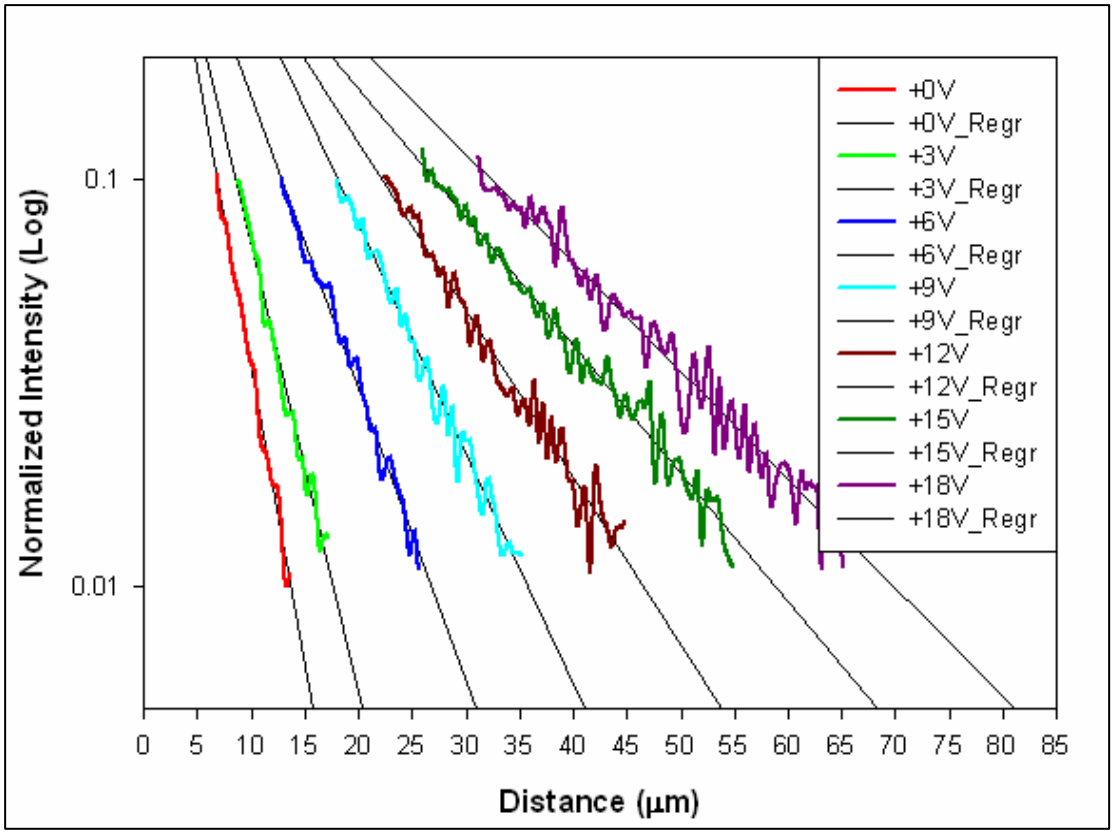

Figure 25 (color) Boone Sample 9 Intensity vs. Distance (Semi-log with regressions).

In the presence of an E field, the modeled slope is as follows:

$$C = \frac{\mu\tau E - \sqrt{(\mu\tau E)^2 + 4\left(\frac{kT}{e}\right)\mu\tau}}{2\left(\frac{kT}{e}\right)\mu\tau} = \left(\frac{e}{2kT}\right)E - \sqrt{\left(\frac{e}{2kT}\right)^2 E^2 + \frac{1}{L_{diff}{}^2}} \qquad (26)$$

where E is the applied E field. Knowing the E field, a measurement of the slope yields the diffusion length by the following:

$$L_{diff} = \sqrt{\left\{\left[\left(\frac{e}{2kT}\right)E - C\right]^2 - \left(\frac{e}{2kT}\right)^2 E^2\right\}^{-1}} \qquad (27)$$

The technique described above for "curve fitting" using the slope of the Intensity vs. Distance on a semi-log plot enables one to estimate the $(\mu\tau)$

product, and thereby the minority carrier diffusion length, with a single drift measurement. However, the accuracy of the estimate depends upon how well the applied E field strength is known.

3. Measurement of the E-field

A four-point measurement was performed on Boone Sample 9 in order to determine the applied E field strength in the region where the drift measurement was performed. Figure 26 is an SEM image of the sample showing the four contacts (A, B, C, D) across which the voltage measurements were made.

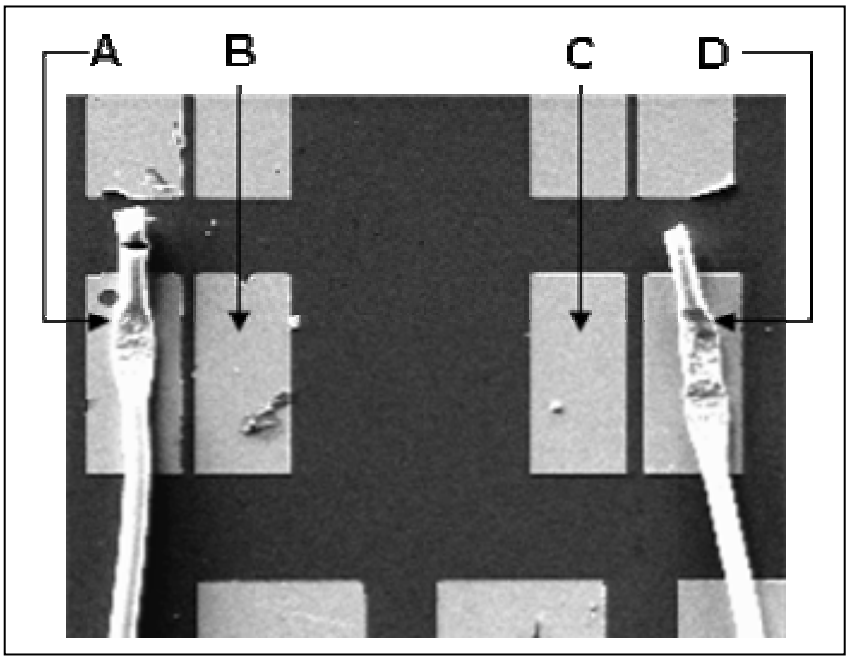

Figure 26 Boone Sample 9 E field measurement area (600 μm x 400 μm).

Each contact in Figure 26 is 80 μm wide; the center-to-center spacing between contacts A and D is 470 μm (x_1) and the center-to-center spacing between contacts B and C is 280 μm (x_2). The gold wires connected to contacts A and D were expertly put down by Jeff Beeman at Lawrence Berkeley National Laboratory. A series of known voltages (-19V to +19V) was applied between contacts A and D and voltage measurements were made between contacts B and C. The measured voltage drop through the material for a known

range of applied voltages divided by the measured distance between the contacts provides precise knowledge of the E field in the region of the transport imaging measurement, as shown in Figure 27.

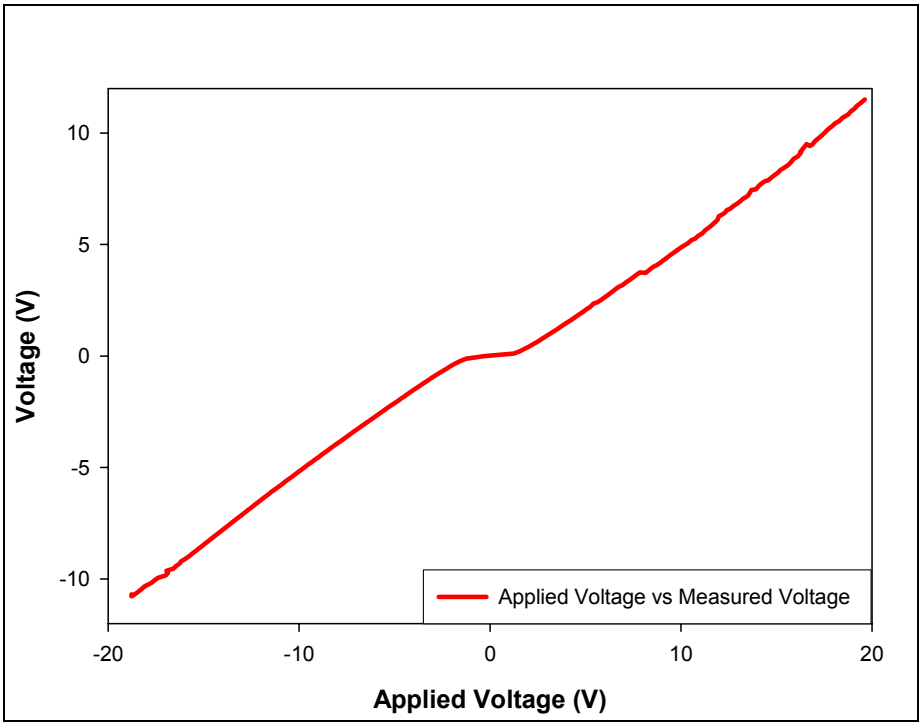

Figure 27 (color) Boone Sample 9 applied voltage from -19 V to +19 V across contacts A and D vs. measured voltage across contacts B and C.

In addition to providing valuable knowledge about the E field strength, comparing the measured voltage drop between contacts B and C to what one would expect from purely geometrical considerations through the material yields an estimation of the voltage drop at the contacts as a function of applied bias. By geometry alone:

$$Voltage(measured) = Voltage(applied)\left(\frac{x_2}{x_1}\right). \tag{28}$$

Figure 28 shows the estimated drop at the contacts for this measurement.

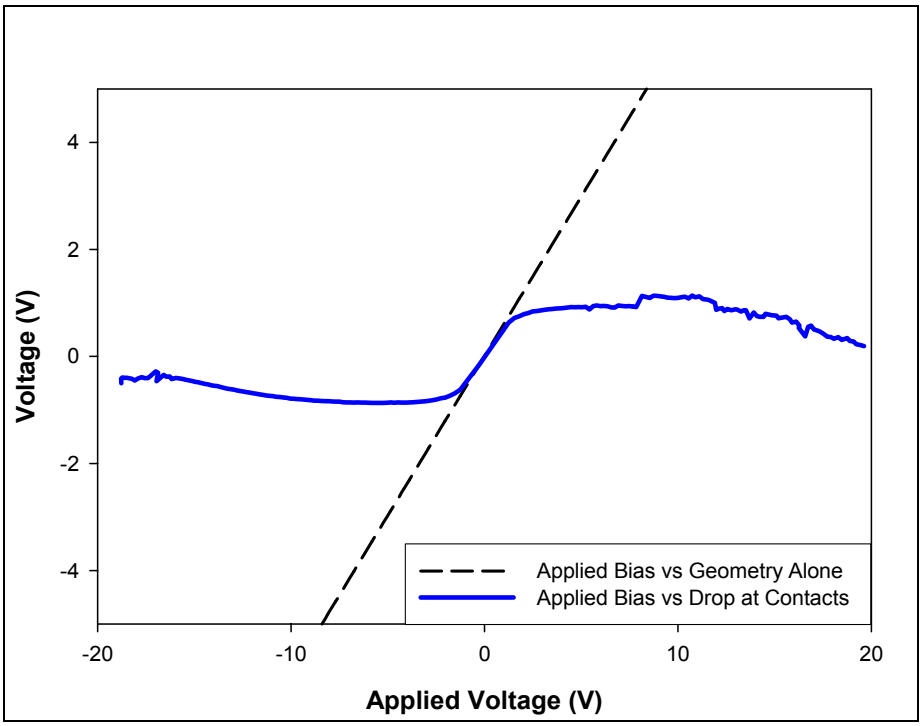

Figure 28 **(color) Boone Sample 9 estimated voltage drop at the contacts by comparing the measured voltage between contacts B and C to geometry alone.**

4. Experimental Results

Using the regression curve slopes from Figure 25 and the E field strength from Figure 27 in Equation (27), the following results were found (Table 1):

Applied Bias:	Measured Bias:	E-field:	Contacts:	Slope:	Diffusion Length:	(μτ)	(μ)
[+V]	[+V]	[V/cm]	[+V]	[1/μm]	[μm]	[cm^2/V]	[cm^2/Vs]
0.00	0.00	0.00	0.00	-0.31	3.2	3.9E-06	9.1E+02
3.00	0.88	44.00	0.86	-0.25	3.1	3.5E-06	8.2E+02
6.00	2.63	131.50	0.94	-0.16	3.0	3.5E-06	8.0E+02
9.00	4.19	209.50	1.13	-0.13	2.9	3.2E-06	7.3E+02
12.00	6.27	313.50	0.87	-0.09	2.9	3.1E-06	7.2E+02
15.00	8.24	412.00	0.76	-0.07	2.9	3.2E-06	7.4E+02
18.00	10.43	521.50	0.33	-0.06	2.8	3.0E-06	7.0E+02

Table 1 **Boone Sample 9 room temperature minority carrier mobility and diffusion length results.**

The transport imaging technique provides a minority carrier diffusion length of approximately 3.0 μm for this sample. Using Equation (12) and the known minority carrier lifetime, the minority carrier mobility is found to be 910 cm^2/Vs for the +0 V bias case. This is in excellent agreement with the value calculated for heavily-doped p-type GaAs ($\sim$ 5 x 10^{18} cm^{-3}) by Bennett [18]. In that work, closed-form analytic expressions derived from quantum mechanical calculations are presented for electron and hole mobilities at 300 K in *p*-type and *n*-type $Ga_{1-x}Al_xAs$ as a function of dopant densities between 10^{16} and 10^{20} cm^{-3} and mole fractions of AlAs with $0.0 \le x \le 0.3$. The minority electron mobility from Table I of that work, following the $x = 0$ line (pure GaAs), yields a value of 990 cm^2/Vs.

THIS PAGE LEFT INTENTIONALLY BLANK

VI. CONCLUSION AND SUGGESTIONS FOR FURTHER RESEARCH

A. SUMMARY AND CONCLUSION

A quantitative method for extracting minority carrier diffusion and drift lengths has been developed and demonstrated in a heavily-doped heterostructure. This method advances the high resolution transport imaging technique, yielding the $(\mu\tau)$ product with a single measurement. A minority carrier diffusion length of approximately 3.0 μm is measured in the 1000 Å-thick active GaAs layer of an AlGaAs/GaAs/AlGaAs heterostructure, modulation-doped p-type with Be at $\sim$ 5 x 10^{18} acceptors/cm^3. The minority carrier mobility is found to be 910 cm^2/Vs, in excellent agreement with the 990 cm^2/Vs theoretical value calculated by Bennett [18]. This is the first demonstration of an SEM-based, contact-free, non-destructive technique for high-resolution minority carrier lifetime measurement.

The imaging transport technique has also been employed to image the nature of the generation region as a function of beam energy, probe current and sample atomic number. In high-Z and low-Z materials, the width of the generation volume increases as a function of increasing e-beam accelerating voltage, in excellent agreement with previous theoretical work. However, we do not observe an increase in linear extent for the low Z material, as might be expected from Monte Carlo calculations. These direct images reveal a relatively narrower generation/recombination volume width for the low-Z than for that of the high-Z material under exactly similar excitation conditions. These types of images should be useful to allow for experimental verification of resolution limits in CL and EBIC associated with interaction volume effects in bulk materials and can be obtained without additional sample preparation.

In conclusion, the high resolution imaging transport technique is advanced to a quantitatively rigorous process to extract key material parameters with a single, non-destructive measurement. This technique can be employed with no

additional sample preparation to any luminescent material. As demonstrated in a heterostructure with ohmic contacts, this method yields experimental minority carrier mobility values that are in excellent agreement with theoretical calculations.

B. SUGGESTIONS FOR FURTHER RESEARCH

1. Electric Field Mapping

Further application of the direct transport imaging technique presented in this work suggests a potentially highly sensitive technique for local E field mapping. As solid-state electronic devices continue to shrink to the micro- and nano-scales, the contacts must operate at ever smaller distances from one another. Therefore, understanding the near-contact E field behavior is essential.

Because the minority carriers are manipulated with an applied E field during transport imaging, the field itself could be directly studied in a material of known parameters, assuming local uniform material properties. In Boone Sample 9, the E field has been quantitatively probed, as presented in the following section. Future efforts should include developing a quantitative method for probing near-contact E fields.

Parallel-plate E fields and E fields of non-standard geometry in Boone Sample 9 have been qualitatively probed using the transport imaging technique. Figure 29 illustrates the geometry of one such non-standard E field probe.

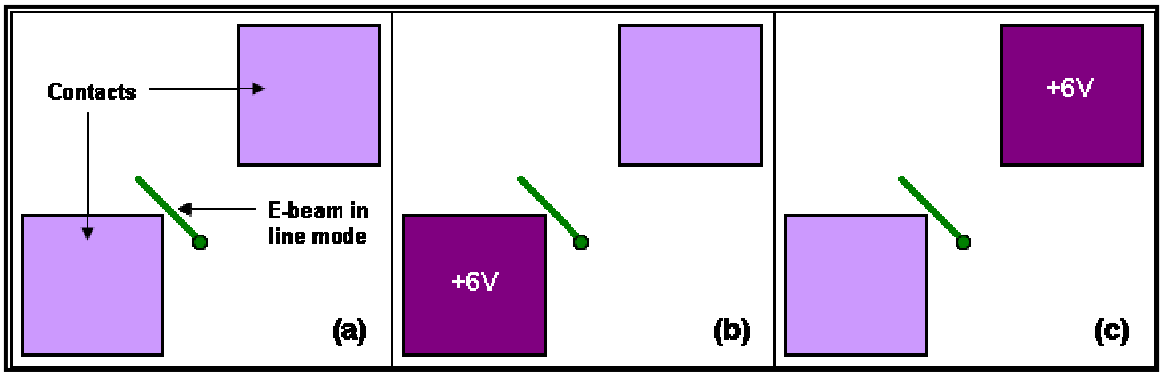

Figure 29 **(color) Geometry of non-standard E field probe. (a) represents the +0V bias case; (b) with a +6V bias on the near contact; (c) reversed polarity.**

First, the SEM is operated in line mode with no applied bias, as depicted in Figure 29(a). The location and orientation of the e-beam with respect to the contacts is represented by the green line. A six volt bias is then applied across the contacts, as in Figure 29(b). Finally, the polarity of the bias is reversed as represented in Figure 29(c). The resulting effect of the non-standard E field on the diffusion and drift of minority charge carriers is seen in the location of their radiative recombination in Figure 30.

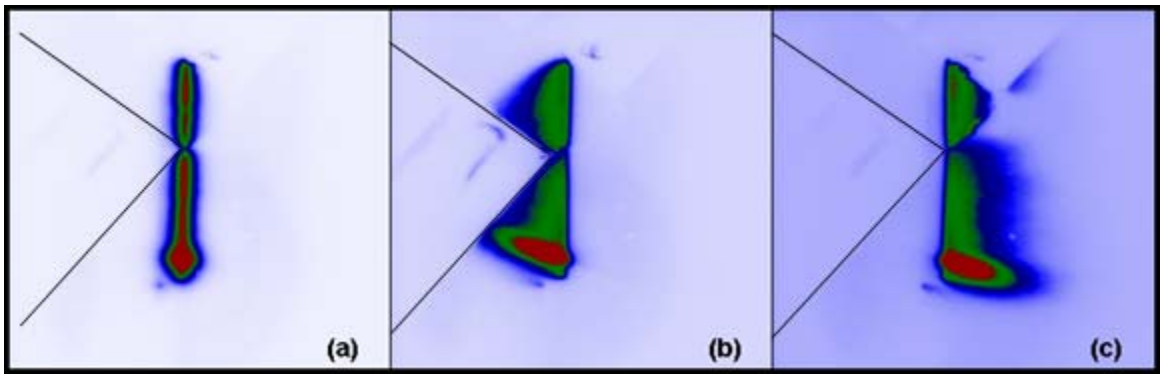

Figure 30 **(color) Results of non-standard E field probe, (a), (b) and (c) correspond to Figure 29 (a), (b) and (c), respectively and are approximately 246 x 261 μm (full area) each.**

In Figure 30, the location of the near contact has been artificially accentuated. Note the way in which the light follows the bending E field lines and changes in intensity as the minority charge carriers diffuse, drift and finally recombine within

the applied E field. As these images suggest, the imaging transport technique is a potentially powerful tool with which to study near-contact E field behavior.

2. Mapping of Radiation Damage in Solar Cells

In addition to studying near-contact E fields, the unique transport imaging technique should be employed to study the effects of radiation damage on the E fields in solar cells. As was discussed in Chapter II, knowledge of the $(\mu\tau)$ product with a high degree of spatial resolution through a simple experimental approach is critical to the solar cell designer. Preliminary transport imaging experiments have been performed on a 1%-In GaInAs (lattice-matched) double-heterostructure solar cell with a 3 μm-thick active layer, doped *p*-type at $\sim$1 x 10^{16} cm^{-3}, with a TRPL-measured lifetime of 2450 ns, as presented in the following section. Future efforts should include developing a quantitative method for characterizing the damage done to solar cell materials by radiation, as well as experimentally extracting key material parameters from new solar cell materials such as InGaN. These new materials are being developed for their radiation-robust properties [20].

Initial transport imaging probes of the double-heterostructure solar cell suggest that fundamentally different phenomena from those in 3D bulk materials and 2D heterostructures may be responsible for the observed minority carrier behavior. For example, Figure 31(a) shows the generation region in the double-heterostructure solar cell produced with a 20keV, 1 x 10^{-9} A e-beam in the absence of any applied voltage bias; in Figure 31(b), a bias of +1.3 V, corresponding to an E field of 162.5 V/cm, has been applied.

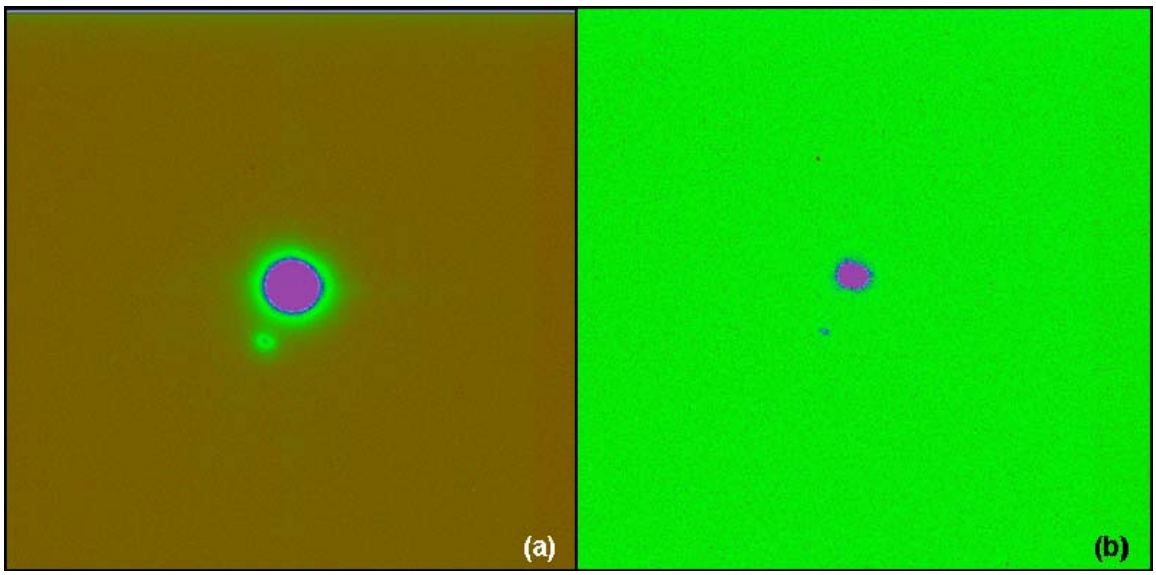

Figure 31 (color) Generation region in a solar cell using a 20keV, 1 x 10^{-9} A e-beam in spot mode, with (a) no applied bias and (b) +1.3 V bias. Each image is ~ 220 μ m x 220 μ m.

Note that no drift tail in the direction of the applied bias is observed, as might be expected from the Boone Sample 9 heterostructure study above. Instead, the intensity has markedly decreased in the presence of the applied field. An observable decrease in intensity as a function of increasing E field was observed, as plotted in Figure 32.

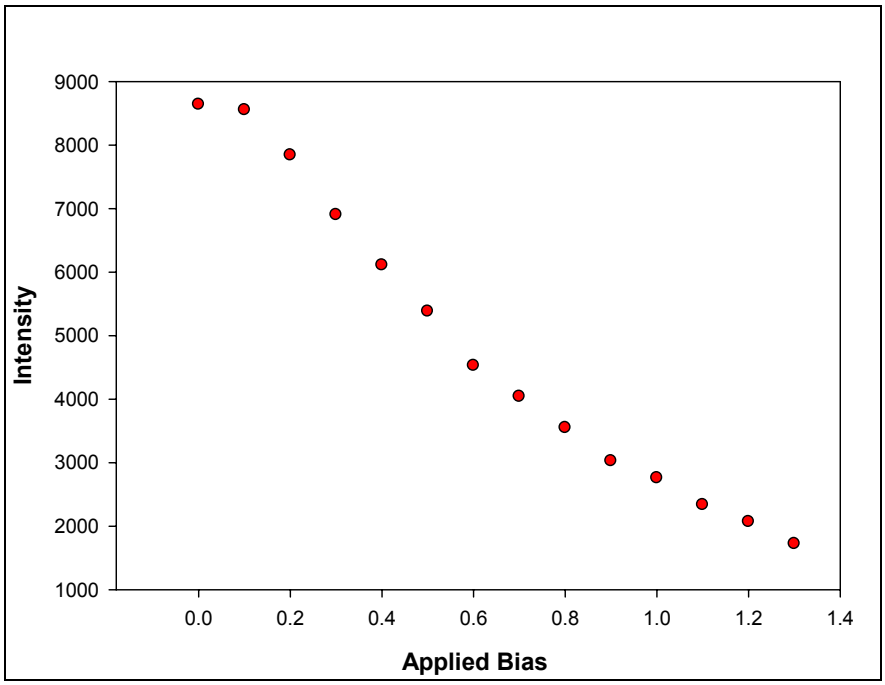

Figure 32 Intensity vs. applied E field in a solar cell using a 20keV, 1 x 10^{-9} A e-beam in spot mode.

Although no drift tail was observed, drift behavior was observed when the SEM was operated in picture mode with the raster area overlapping either contact, the geometry of which is illustrated in Figure 33.

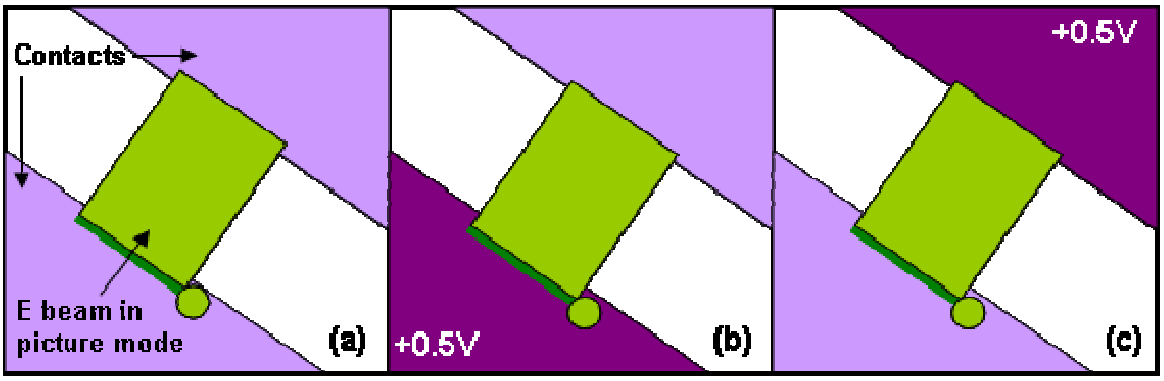

Figure 33 (color) Geometry of solar cell drift probe using the SEM picture mode. (a) represents the +0V bias case; (b) with a +0.5 V bias on the lower-left contact; (c) reversed polarity.

First, the SEM is operated in picture mode with no applied bias, as depicted in Figure 33(a). The location and orientation of the e-beam with respect to the contacts is represented by the green region. An 0.5 V bias is then applied across the contacts, corresponding to an E field of 62.5 V/cm, as in Figure 33(b). Finally, the polarity of the bias is reversed as represented in Figure 33(c). The resulting effect of the applied E field on the diffusion and drift of minority charge carriers within the interaction region is seen in Figure 34.

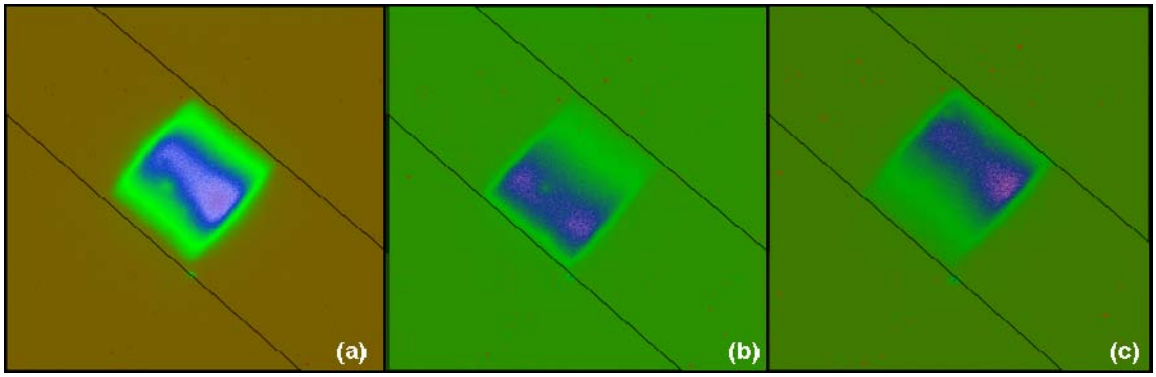

Figure 34 (color) Generation region in a solar cell using a 20keV, 1 x 10^{-9} A e-beam in picture mode, with (a) no applied bias, (b) +0.5 V bias on the lower-left contact and (c) reversed polarity. Each image ~ 220 μm x 220 μm. Inter-contact distance ~ 80 μm.

In Figure 34, the location and orientation of the contacts have been artificially accentuated. Note the shift in peak intensity within the interaction region with the application and subsequent reversal of polarity of an applied E field. Further studies are needed to understand this behavior and advance the imaging transport technique to a quantitative measurement tool for these solar cells. Once this goal is achieved, differences between pristine and radiation-damaged solar cells can be experimentally sought and the degree to which a solar cell is damaged by or hardened against radiation can be quantitatively characterized.

3. Low-dimensional Structure Studies

Results of experiments performed to date on the low-dimensional double-heterostructure solar cell and a superlattice sample (20 X 100 Å-thick active GaAs layers between AlGaAs layers, modulation-doped p-type with Be at ~ 5 x 10^{18} acceptors/cm^3) are not yet understood. However, they do suggest an exciting possibility: the low-dimensional geometry of the active layers of these structures may be giving rise to observable changes in charge carrier transport properties. If found, this would open the door for the creation of low-dimensional semiconductor devices whose minority charge carrier parameters may be controllable by an E field, facilitating extremely fast switching and tremendous packing densities. Further experiments performed with nano-scale resolution provided by the new SEM hardware on order in our laboratory in conjunction with the installed beam-blanker should facilitate the understanding of minority charge carrier transport properties of low-dimensional structures such as superlattices and quantum wires, which are poised to usher-in the next revolution in solid-state electronic devices.

LIST OF REFERENCES

1. Yacobi, B.G. and D. B. Holt, *Cathodoluminescence Microscopy of Inorganic Solids* (Plenum, New York, 1990).

2. Haegel, N.M., J. D. Fabbri and M. P. Coleman, *Appl. Phys. Lett.* **84**, 8 (2004).

3. Liboff, R.L., *Introductory Quantum Mechanics*, fourth edition (Addison Wesley, San Francisco, 2003).

4. Kasap, S.O., *Optoelectronics and Photonics, Principles and Practices* (Prentice Hall, New Jersey, 2001).

5. Kasap, S.O., *Principals of Electronic Materials and Devices* second edition (McGraw Hill, New York, 2002).

6. Gustafsson, A., M. E. Pistol, L. Montelius and L. Samuelson, *J. Appl. Phys.* **84**, 1715 (1998).

7. Haynes, J.R. and W. Shockley, *Phys. Rev.* **81**, 835 (1951).

8. Stan, M.A., P.R. Sharps, N.S. Fatemi, F. Spadafora, D. Aiken and H.Q. Hou, 0-7803-5772-8, *IEEE* (2000).

9. Olsen, R.C. "Introduction to the Space Environment" Course Notes, Naval Postgraduate School, Monterey, CA, June 2003.

10. Kayana, K. and S. Okayama (1972), *J. Phys. D Appl. Phys.* **5**, 43.

11. Goldstein, J., Dale Newbury, David Joy, Charles Lyman, Patrick Echlin, Eric Lifshin, Linda Sawyer and Joseph Michael, *Scanning Electron Microscopy and X-Ray Microanalysis, Third Edition* (Plenum, New York, 2002).

12. Donolato, C. and P. Venturi, *Phys. Stat. Sol. (a)* **78**, 377 (1982).

13. Everhart, T.E., R.F. Herzog, M.S. Chang and W.J. DeVore (1972). In *Proceedings of the 6th International Conference on X-Ray Optics and Microanalysis* (G. Shinoda, K. Kohra and T. Ichinokawa, eds.), University of Tokyo Press, Tokyo, p. 81.

14. Araujo, D., J. M. Bonard, G. Oelgart, J. D. Ganiere, F. Morier-Genoud and F. K. Reinhart, *Mater. Sci. Eng. B* **24**, 124 (1994).

15. Bonard, J.M., J. D. Ganiere, B. Akamatsu, D. Araujo and F. K. Reinhart, *J. Appl. Phys.* **79**, 11 (1996).

16. Werner, U., F. Koch and G. Oelgart, *J. Phys. D*, **21**, 116 (1988).

17. Boone, T.D., H. Tsukamoto, J. M. Woodall, *Appl. Phys. Lett.*, **82**, 19 (2003).

18. Bennett, H.S., *Journal of Applied Physics* **92**, 8 (2002).

19. Boaz, M.L., Mathematical Methods in the Physical Sciences, Second Edition (John Wiley and Sons, 1983) (pg 525).

20. Wu, J., W. Walukiewicz, K. M. Yu, W. Shan, J.W. Ager III, E. E. Haller, H. Lu, W. J. Schaff, W. K. Metzger and S. Kurtz, *J. Appl. Phys.* **94**, 10 (2003).

INITIAL DISTRIBUTION LIST

1. Defense Technical Information Center
   Ft. Belvoir, Virginia

2. Dudley Knox Library
   Naval Postgraduate School
   Monterey, California

3. Marine Corps Representative
   Naval Postgraduate School
   Monterey, California

4. Director, Training and Education, MCCDC, Code C46
   Quantico, Virginia

5. Director, Marine Corps Research Center, MCCDC, Code C40RC
   Quantico, Virginia

6. Marine Corps Tactical Systems Support Activity (Attn: Operations Officer)
   Camp Pendleton, California

7. Head, Information Operations and Space Integration Branch,
   PLI/PP&O/HQMC
   Washington, DC

8. Professor James H. Luscombe
   Naval Postgraduate School
   Monterey, California

9. Professor James H. Luscombe
   Naval Postgraduate School
   Monterey, California

10. Professor Rudy Panholzer
    Naval Postgraduate School
    Monterey, California

11. Professor Nancy M. Haegel
    Naval Postgraduate School
    Monterey, California

12. Professor Sherif Michael
    Naval Postgraduate School
    Monterey, California

13. Dr. Tom Boone
Hitachi Global Storage
San Jose, California

14. David R. Luber
PLI/PP&O/HQMC
Washington, DC